



Springs and streams of the Taro–Ceno Valleys (Northern Apennine, Italy): Reaction path modeling of waters interacting with serpentinized ultramafic rocks

Tiziano Boschetti*, Lorenzo Toscani

Earth Sciences Department, University of Parma, v.le G.P. Usberti 157/A, I-43100 Parma, Italy

ARTICLE INFO

Article history:

Received 6 May 2008

Received in revised form 18 August 2008

Accepted 19 August 2008

Editor: J. Fein

Keywords:

Ultramafic rocks

Poorly crystalline serpentine

Reaction-path modeling

Bicarbonate waters

Alkaline waters

ABSTRACT

In the area of the Taro–Ceno Valleys (Northern Apennine, Emilia-Romagna region, Italy), waters of meteoric origin interact with ophiolite rocks of the External Ligurides. Fresh water springs issuing from basalts have a Ca–HCO₃ composition, whereas freshwater springs from ultramafites vary in composition from Ca–HCO₃ or Mg–HCO₃ to Na–OH or Na–SO₄ types and in pH values from 7.3–8.8 up to pH 11, respectively. In addition, the boron content of the alkaline waters is up to 13 mg/L, which is unusually high for freshwaters in general and ultramafites that have undergone oceanic serpentinisation in particular and gives a boric alkalinity to the waters. The springs waters show evidence of recent low-temperature continental serpentinisation and the process is modeled by reaction paths using an updated geochemical thermodynamic database, consistent with the local primary and secondary serpentinite paragenesis. For the model, bicarbonate waters evolve to alkaline waters supersaturated in Ca–(Mg)-carbonate, based on the assumption that the dissolution of serpentinite results in supersaturation with respect to kaolinite, ferrihydrite, vermiculite, Fe²⁺–Mg²⁺–saponite, and poorly crystalline serpentine. The alkaline composition and the chloride content of the waters suggest a prolonged interaction with the rocks at depth that led to dissolution of albite and leaching of olivine-hosted fluid inclusions. A similar evolution is also proposed for the more developed springs issuing from the ultramafic rocks of the Voltri Group (Liguria region), where solutions are supersaturated in brucite and are in equilibrium with enstatite and/or chlorite.

© 2008 Elsevier B.V. All rights reserved.

1. Introduction

Many studies have reported the ubiquity of magnesium-bicarbonate and calcium-hydroxide spring waters that are associated with ultramafic rocks and that originated from meteoric water (e.g. Barnes et al., 1967, 1972, 1978; Barnes and O'Neil, 1969; Pfeifer, 1977; Bruni et al., 2002). According to Neal and Stanger (1984), these waters can promote serpentinization at low temperature, for example in the Oman ophiolite, where up to 10% of serpentines are estimated to be supergenic. Other authors (Pfeifer, 1977; Birsoy, 2002; Bruni et al., 2002; Marini and Ottonello, 2002) have downplayed the formation of serpentines during weathering of ultramafic rocks; these investigators consider the precipitation of sepiolite to be the dominant process. Lapham (1961) named *deweylite* the poorly crystalline serpentine that precipitates from colloidal suspensions at low temperature. Nevertheless, researchers rarely study these serpentine-like mineraloids in the field or laboratory, since poorly crystalline material is regarded with suspicion. Thus, these mineraloids are not used to define the crystallographic, chemical, or structural details of serpentine minerals. In the Northern Apennine, possible protoserpentine analogues,

genetically comparable with the microstructures forming mesh and bastites, have been found and described (e.g. Mellini and Zanazzi, 1987; Viti and Mellini, 1998). In the late 1970s, hydrogen isotopes confirmed the low-to-medium temperature origin (25–185 °C) of some chrysotile and lizardite minerals (Wenner and Taylor, 1974). More recently, in order to estimate the expected δ¹⁸O–δ²H isotopic composition of continental serpentine formed in equilibrium with meteoric water at 25 °C, Kyser et al. (1999) and Barnes et al. (2006) inferred a “serpentine–H₂O (25 °C)” line. Further, the occurrence of highly deuterium depleted hydrogen gas emanating from hyperalkaline discharges also was used as an indication of “low temperature” serpentinization (Neal and Stanger, 1983). However, the isotopic evidence of continental-meteoric low temperature serpentinization remains scarce. This paucity of data may reflect a fairly low water/rock ratio during the process and, consequently, an oxygen isotope composition of serpentines largely inherited from precursor minerals (Barnes et al., 1978).

Water–rock interaction modeling of Ca–OH waters is difficult, particularly when the detailed composition and thermodynamic parameters on the rock-forming minerals are unavailable (O'Hanley, 1996). For example, in spite of the importance of vermiculite in weathering processes (Lee et al., 2003), models in the literature have ignored their role for lack of thermodynamic data. Other factors that play fundamental roles in controlling the serpentinite

* Corresponding author. Present address: via Stradone 658, 47030 – S. Mauro Pascoli (FC), Italy. Tel.: +39 3470186527; fax: +39 0521 905305.

E-mail address: work@tizianoboschetti.com (T. Boschetti).

supergenic mineralogy are the dissolution-precipitation kinetics (Nesbitt and Bricker, 1978; Siever and Woodford, 1979) and climate (Wrucke, 1996).

In this study, the chemical and isotopic composition of several spring waters issuing from different outcrops of ophiolitic rocks in the Parma Province (Toscani et al., 2001; Boschetti, 2003), are presented and modeled for fluids circulating in and interacting with ultramafic rocks of the Northern Apennine. The model shows the role of primary and secondary minerals in the reaction path. Solubility products specific for local phases were calculated and inserted in the modeling, and the role of low-temperature serpentine in the chemical evolution of groundwater from the Taro–Ceno Valleys and the Voltri Group area (Bruni et al., 2002; Marini and Ottonello, 2002) is discussed.

2. Geological and hydrogeological setting

The geology and petrology of Northern Apennine ophiolites (ultramafites, basalts, and cherts) have been extensively investigated (Abbate et al., 1980; Beccaluva et al., 1984; Ottonello et al., 1984; Rampone et al., 1995, 1996). Most researchers agree that the ophiolites (i) were generated in the Piedmont–Ligurian ocean during the Jurassic and Cretaceous periods, (ii) are remnants of the ocean crust and

overlying sediments, (iii) were fragmented into several nappes during the Upper Cretaceous–Eocene stage of the orogeny, and (iv) reflect the fact that the entire allochthonous pile overrode the continental crust during the Oligocene and Miocene periods.

The Northern Apennine ophiolites crop out in two palaeogeographic domains: the Internal Ligurides (IL) and External Ligurides (EL), which are identified on the basis of their current structural characteristics and their relationship with the associated sedimentary sequences (Abbate et al., 1980, and references therein). IL contains strongly depleted peridotites, serpentinites, gabbros, and basalts (N-MORB), which are the basis of the Upper Jurassic–Paleocene sedimentary sequence, i.e. deposits of Mn ore associated with radiolarian cherts, silicic limestones, Palombini shales with limestones. EL, on the other hand contains less depleted lherzolites in association with E-MORB (Ottonello et al., 1984; Beccaluva et al., 1984; Rampone et al., 1995, 1996). In the Taro–Ceno river valleys, springs issuing from ophiolite rocks occur in three areas (Fig. 1): (A) Mt. Penna–Mt. Aiona and Mt. Maggiorasca–Mt. Nero, where the Taro river and the Ceno stream have their sources; (B) the areas around the Belforte, Val Manubiola, and Valmozzola along the middle course of the river; and (C) Mt. Prinzerza, where the Taro River enters the Po Plain.

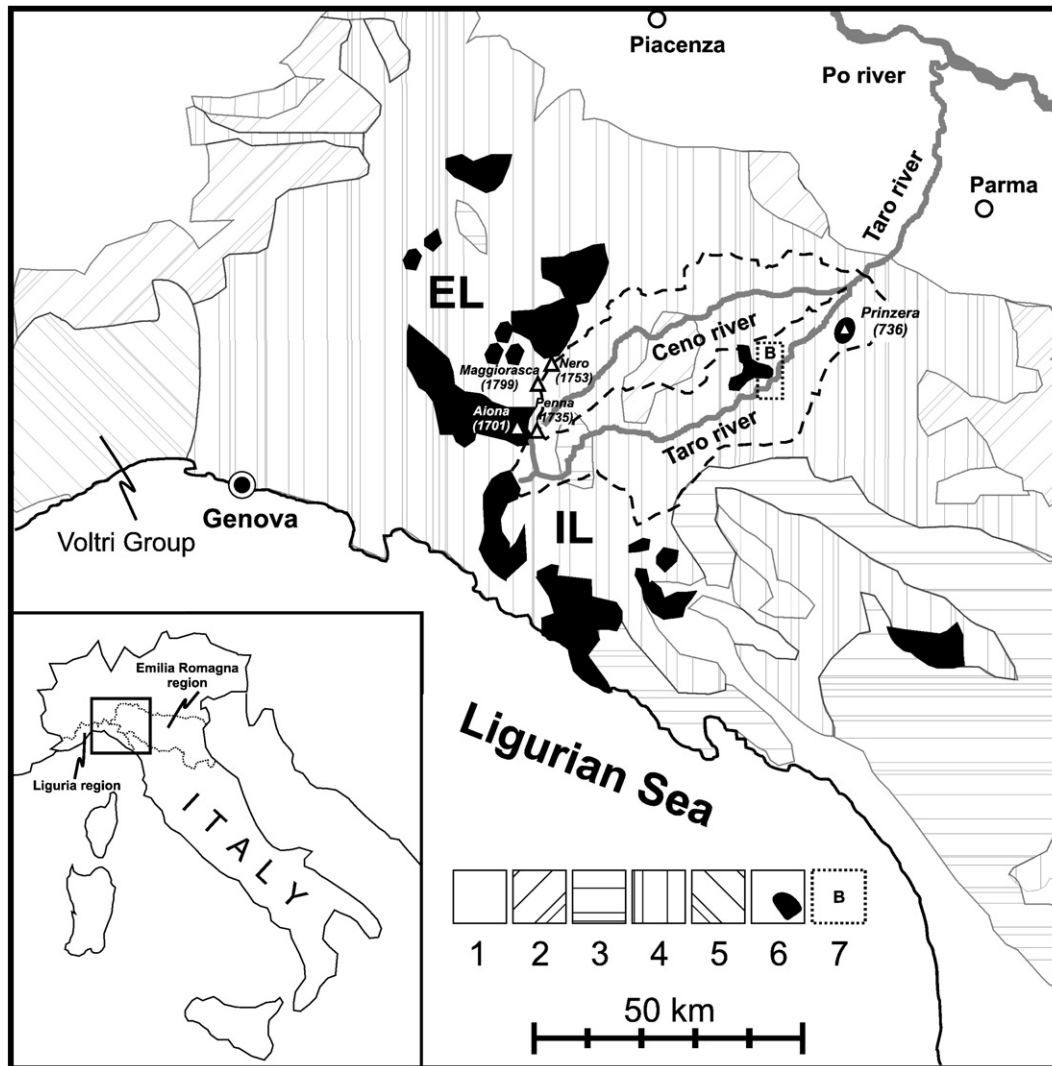


Fig. 1. Simplified geologic map of the Northern Apennine (modified from Beccaluva et al., 1984). The samples of this study are located in the Taro–Ceno Valleys (sketched outline). 1 = Messinian to present; 2 = paraautochthonous and Piemontese Tertiary; 3 = Tuscan–Umbrian sequences; 4 = ophiolites and sedimentary sequences of the Liguride units; 5 = high-pressure metamorphic ophiolites and calcschists of the Alpine Units; 6 = Ligurides ophiolitic masses (EL = External Liguride unit; IL = Internal Liguride unit); 7 = Middle Taro “area B” sampled: Belforte–Val Manubiola–Valmozzola. White triangles: mountains cited in the text, with altitude in brackets (meters a.s.l.).

Basaltic rocks, which are absent only from the area of Mt. Prinzer, suffered an early low-grade oceanic metamorphism to varying extents, followed by an orogenic metamorphism (Cortesogno, 1980). Albite, epidote, prehnite, sericite, chlorite, actinolite, titanite, and haematite association replaced the original mineralogy of plagioclase, olivine, clinopyroxene, ilmenite, and magnetite (Cortesogno and Lucchetti, 1982). Spinel lherzolites re-equilibrated in the petrological field of plagioclase lherzolites and were exposed to oceanic and orogenic metamorphisms. Hydration of the early mineralogy produced serpentine (lizardite and minor chrysotile), chlorite, and talc and bastite after olivine and orthopyroxene, respectively.

The ultramafites of the Middle Taro valley and of Mt. Prinzer are strongly serpentinized (Venturelli et al., 1997), whereas primary clinopyroxene and plagioclase are largely preserved at Mt. Aiona (Beccaluva et al., 1973). Sedimentary rocks at the contacts with the ophiolites are predominantly flyschoid (marly to pelitic) and arenaceous. Typically, flysch rocks are micritic marly turbidites with interbedded pelites; at Mt. Caio the latter are composed of illite, and/or illite/smectite mixed layers and chlorite (Venturelli and Frey, 1977). Arenaceous formations include (i) the Casanova Complex, composed of quartz-feldspathic rocks with metamorphic, serpentinitic, and volcanic clasts (Di Giulio and Geddo, 1990); and (ii) the Ostia Sandstones, composed of quartz, feldspar (plagioclase, orthoclase, microcline), mica (muscovite, biotite), calcite, and dolomite within a clayey and chlorite matrix at the base of the Mt. Caio Flysch Formation (Mezzadri, 1964).

Hydrogeologic studies on the Taro–Ceno Valleys were focussed on their alluvial fan and plain, probably because they cover a densely populated area. Recently, research projects consider the upstream section of the valleys and preliminary results show that 77% of the springs are fed by aquifers contained in Late Cretaceous Ligurian flysch, 11% in sandstones–pelite, conglomerates and massive sandstones (e.g. Ranzano Formation) and only 4% in ophiolitic bodies (Segadelli et al., 2006; De Nardo et al., 2007). According to the authors, the last value is probably underestimated because the study considers only the known and gathered springs for waterwork system, whereas most of springs issuing from ophiolites are free and unknown, despite their perennial activity that ensure preservation of the stream outflow during dry periods. De Nardo et al. (2007) identify two types of ophiolite related springs: (i)

springs with indefinite permeability limit and (ii) with definite permeability limit which are fed by aquifers contained in fractured rocks and in coarse detritic covers respectively. Some high flow rate springs have different origin being related to gravitational sliding (e.g. Mt. Nero area) that increased permeability due to slackening of the pre-existing fractures (De Nardo et al., 2007).

3. Analytical methods

3.1. Field methods

All water samples were filtered through cellulose acetate filters (0.45 µm). An aliquot for cation analysis was acidified with 65% HNO₃ Suprapur Merck (1 cm³ HNO₃ per 100 cm³ water). Labile parameters (temperature, pH, and Eh) were determined in the field using an ORION 250A instrument equipped with a Ross glass electrode for measuring pH and a combined electrode of platinum–silver/silver chloride for measuring Eh. The electrode for Eh was calibrated at different temperatures using ZoBell's solution (Nordstrom, 1977). Specific conductance at 20 °C was measured using a conductimeter (Model 85, Yellow Springs Instruments). Total alkalinity was determined in the field by acidimetric titration with 0.01 N HCl using bromocresol green as an indicator, and in the laboratory by Gran titration (Gran, 1952) within 12 h of sampling. Reduced dissolved species were determined by spectrophotometry using a portable photometer (Merck SQ300) with Spectroquant kits: total ammonium, NH₄ = NH₄⁺ + NH₃, and total sulphide, HS = H₂S⁰ + HS⁻ + S²⁻, were determined by adding indophenol blue in basic solution (pH ≈ 13; method 4500-NH₃ F in APHA-AWWA-WEF, 1995) and methylene blue in acidic solution (pH ≈ 0.5; method 4500-S²⁻ F in APHA-AWWA-WEF, 1995), respectively.

3.2. Laboratory methods

Cl⁻, NO₃⁻, and SO₄²⁻ were analyzed by ion chromatography using Dionex DX100 with anionic self-regenerating suppressor, silica by spectrophotometry using a Merck SQ300 photometer; and Na, K, Ca, Mg, B, Fe, by radial/sequential inductively coupled plasma optical emission spectrometry (ICP-OES) using Philips PU7450 and Horiba Jobin-Yvon Ultima 2 instruments. Data on δ²H(H₂O) and δ¹⁸O(H₂O)

Table 1
Summary of physico-chemical parameters and concentrations of chemical constituents in the spring waters coming from ultramafites and basalts in the Taro–Ceno Valleys

Type (lithology) facies (N samples)	Springs (ultramafites)										Springs (basalts)						
	Ca-bicarbonate (5)					Mg-bicarbonate (15)					Na-OH	Na-SO ₄	Ca-bicarbonate (14)				
Statistic or code	Median	Mean	S.D.	Max	Min	Median	Mean	S.D.	Max	Min	*PR10	*UM15	Median	Mean	S.D.	Max	Min
Temperature (°C)	12.3	12.1	2.7	15.5	8.7	11.4	10.8	3.40	12.6	5.4	11.8	13.3	10.1	8.9	3.3	13.7	4.7
Cond. 20 °C (mS/cm)	310	361	206	581	129	144	218	211	877	92	237	386	73.5	182	252	972	53
Eh (mV)	436	434	34	470	392	445	446	42.2	513	362	-47.6	-9.99	460	467	29	514	423
pH (at T water)	7.81	7.89	0.57	8.80	7.26	7.85	7.82	0.38	8.83	7.27	10.85	10.37	7.21	7.25	0.27	7.70	6.67
tAlk (mg/L as HCO ₃ ⁻)	249	261	157	420	81	98	144	139	618	64.4	61	93	39	87	97	305	25
Cl ⁻ (mg/L)	5.4	5.1	1.0	6.1	3.6	3.6	3.9	1.83	10.0	2.3	19	14	3.6	19	58	222	2.6
SO ₄ ²⁻ (mg/L)	12	19	14	36	5.0	11	21	24	77	2.8	8.9	93	5.4	9.9	9.8	34	3.8
HS (mg/L)	<0.02	<0.02	-	-	-	-	-	-	-	-	0.62	0.56	<0.02	<0.02	-	-	-
NO ₃ ⁻ (mg/L)	4.8	4.8	5.4	8.6	1.0	1.4	2.0	2.22	8.8	0.3	<0.5	<0.5	2.5	2.2	0.7	2.9	1.0
NH ₄ ⁺ (mg/L)	<0.02	<0.02	-	-	-	-	-	-	-	-	<0.06	0.28	<0.02	<0.02	-	-	-
SiO ₂ (mg/L)	14	16	7.7	26	6.9	17	16	5.9	25	0.89	1.5	1.4	6.6	7.2	2.5	15	5.4
Ca (mg/L)	47.8	58.9	35.5	101	19.6	7.5	12.0	17.0	71	1.5	9.1	22.6	12.3	25.8	29.9	97.6	7.2
Mg (mg/L)	24.5	21.8	14.5	38.0	4.5	16.2	24.8	17.1	74.9	11.5	0.14	0.31	2.6	5.4	9.3	37	1.7
Na (mg/L)	5.3	7.4	5.5	15	2.3	1.7	4.5	7.1	28.7	1.0	29	58	2.4	9.9	25.2	97	1.9
K (mg/L)	1.70	1.42	0.93	2.60	0.30	0.26	1.5	4.60	17.5	0.06	0.38	8.93	0.32	0.48	0.44	1.76	0.10
Hard (mg/L)	220	237	146	386	67	90	132	110	486	59	23	58	39	87	105	362	26
TDS (mg/L)	245	263	155	424	84	108	154	133	596	76	100	246	52	124	164	633	41
B (mg/L)	148	161	24	189	147	198	278	177	586	157	2116	13420	91	133	118	363	29
Fe (mg/L)	4.9	7.0	5.7	11	2.9	34	89	96	200	32	3.0	6.4	3.7	50.02	94	191	1.7

- = not analyzed; * = average data from three sampling campaigns; Hard (hardness as CaCO₃) = 2.497 × Ca + 4.118 × Mg (mg/L).

TDS (total dissolved solids) = 0.5 × tAlk + Ca + Mg + Na + K + Cl + SO₄ + (2.82 × H₂S) + NO₃ + (1.02 × SiO₂) (mg/L) (modified after APHA-AWWA-WEF, 1995).

were collected using an automatic equilibration device (Finnigan GLF 1086) in-line with a mass spectrometer (Finnigan Delta Plus). The analyzed H₂ and CO₂ gases were equilibrated with water samples at a temperature of 18 °C (Epstein and Mayeda, 1953) using a Pt-rich catalyst. Isotopic ratio are reported in per mill relative to V-SMOW, and standard errors for δ²H(H₂O) and δ¹⁸O(H₂O) are approximately ± 1.0‰ and within ±0.1‰, respectively.

4. Chemical and isotopic results

The chemical compositions of the waters from the ultramafites and basalts are summarized in Table 1. Complete chemical and isotope data are reported in Appendix A, where all the water samples are subdivided into four classes on the basis of the lithology present at the source: (i) ultramafic, (ii) basaltic, (iii) sedimentary, and (iv) surface waters.

4.1. Chemical classification

All the samples investigated were freshwater (TDS < 1 g/L). The ternary classification diagrams (Na+K)–Ca–Mg and tAlk–SO₄–Cl (Fig. 2) show that waters of groups (ii), (iii), and (iv) do not differ significantly; many are bicarbonate-calcic with neutral to slightly basic pH values (6.67–8.57), highly oxidized (Eh = 371–514 mV), and contain a small amount of chloride (Cl⁻ up to 6.4 mg/L). Sample UM1 from basalt is an exception since it is a Cl–Ca–Na type with EC up to 1043 μS cm⁻¹, Cl⁻ up to 231 mg/L, hardness up to 367 mg/L CaCO₃. Waters issuing from ultramafites have more varied compositions. They range from Ca-bicarbonate, with a pH of 7.3–8.8 and a hardness ranging from moderately hard to very hard (67–386 mg/L CaCO₃; Eh, 129–581 μS cm⁻¹) to Mg-bicarbonate, with a pH of 7.4–8.8 and a hardness from soft to very hard (59–206 mg/L CaCO₃; 92–330 μS cm⁻¹). Among the Mg-bicarbonate waters, sample UM8 shows the highest hardness values

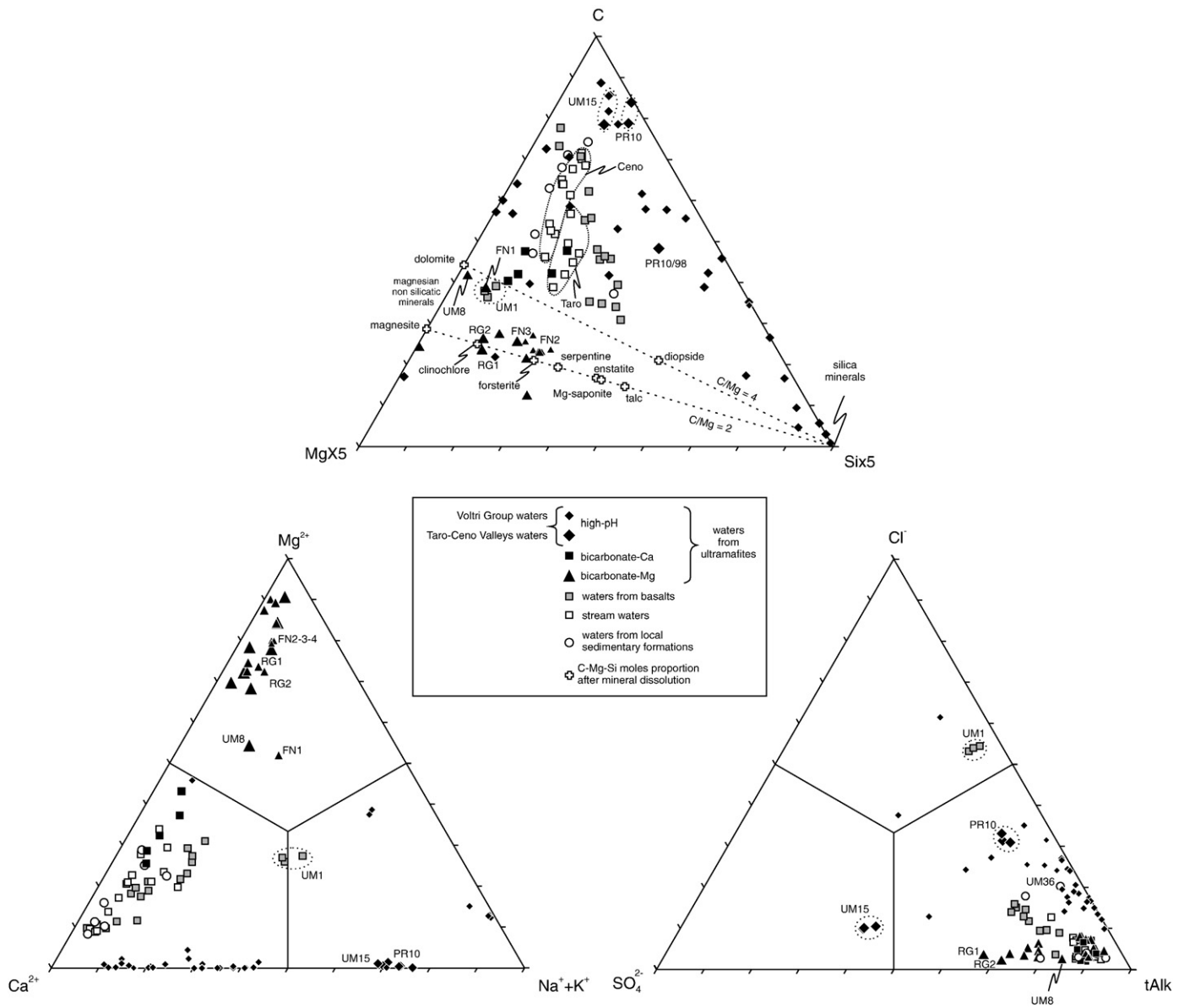
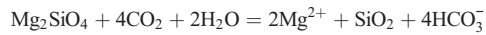


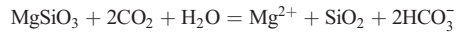
Fig. 2. Mg–Si–C ternary diagram (in mol/kg) and ternary classification diagrams [Mg–(Na+K)–Ca plus Cl–tAlk–SO₄ in meq/L] of alkaline springs in the Taro–Ceno Valleys (this work) and the Voltri Group (Marini and Ottonello, 2002). Bottled waters from Taro valley are also represented: RG1 and RG2, Rocca Galgana 1990 and 1994, respectively (chemical data from water bottle label); FN1, FN2, and FN3, Fontenova 1974, 1990, and 1994, respectively (chemical data taken from water bottle label). Mg–Si–C contents after mineral dissolution (white crosses) are also represented (see text for details). Note that for dolomite and magnesite, the C/Mg mole ratio refers to the products of the respective reactions CaMg(CO₃)₂+2H₂O+2CO₂=Ca²⁺+Mg²⁺+4HCO₃⁻ and MgCO₃+H₂O+CO₂=Mg²⁺+2HCO₃⁻.

(486 mg/L CaCO_3), conductivity ($877 \mu\text{S cm}^{-1}$), and alkalinity (618 mg/L HCO_3^-). Springs PR10 and UM15 from ultramafites show an extreme composition being sodium-hydroxide and sodium-sulfate, respectively; their pH is high (10.1–11.2), their Eh is low (down to -103 mV), they are soft (20–61 mg/L CaCO_3 , 220 to $408 \mu\text{S cm}^{-1}$), and they contain large amounts of boron (up to $2294 \mu\text{g/L}$ and up to $13461 \mu\text{g/L}$, respectively) and moderate amounts of reduced sulfur and nitrogen species. In both PR10 and UM15, non-carbonate alkalinity predominates over carbonate alkalinity: using PHREEQCI software with the *llnl.dat* thermodynamic database (Parkhurst and Appelo, 1999) to calculate the composition of alkaline species under the pH, Eh, and T values measured in field, sample PR10 was found to contain 54% hydroxide, 23% carbonate, 19% borate and 4% other alkaline species (Si, sulphide, and ammonia), while sample UM15 contained 75% borate, 14% hydroxide, 10% carbonate, and 1% other species.

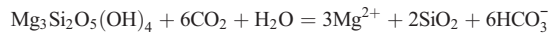
The Si–Mg–C diagram (Fig. 2) is a useful tool for studying water–rock interactions. Dissolution reactions of typical magnesium minerals of ultramafic rocks are represented by a line with $\text{C/Mg}=2$ (molar ratio):



(forsterite)



(enstatite)



(serpentine)

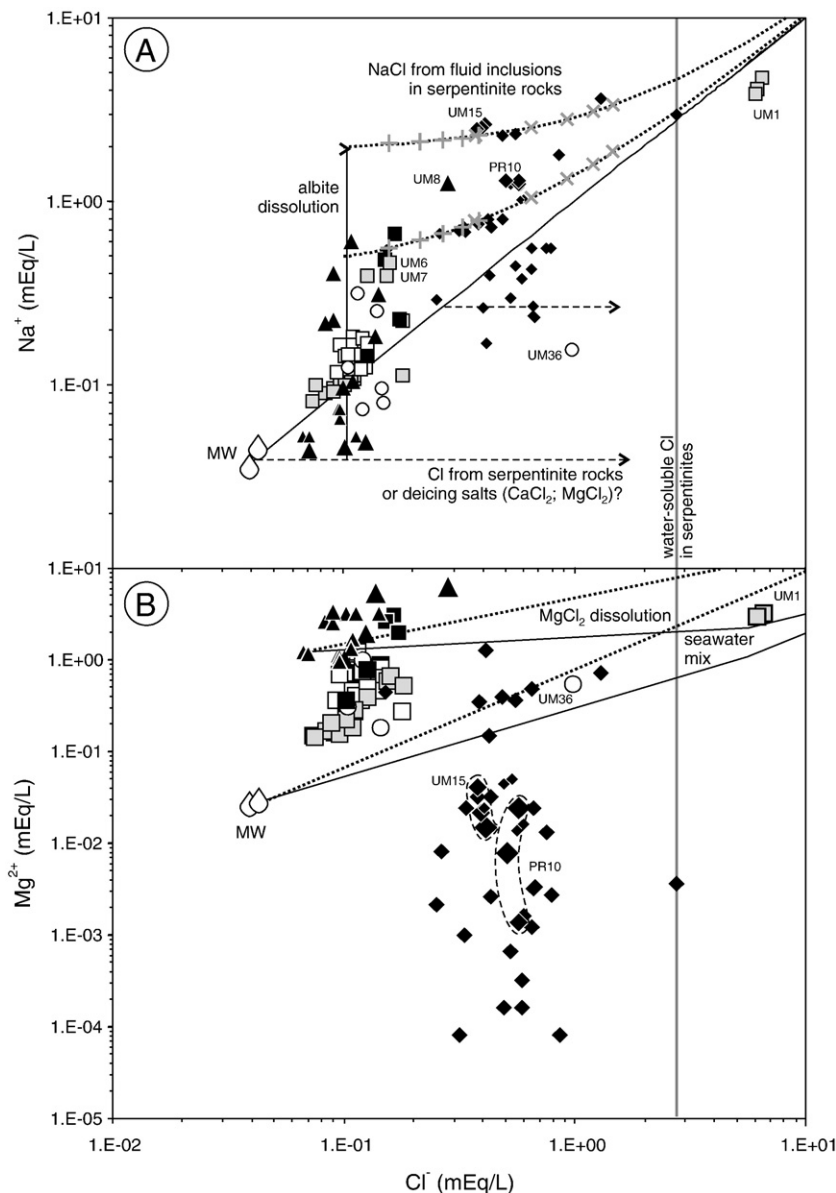
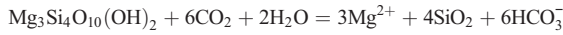
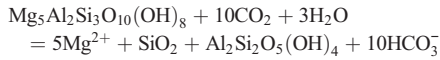


Fig. 3. Plot of (A) Na and (B) Mg vs. Cl for all water samples from the Taro–Ceno Valleys, including bottled waters Rocca Galgana and Fontenova (chemical data taken from labels). Alkaline springs from the Voltri Group (small black diamonds; Marini and Ottonello, 2002) and meteoric water mean composition (MW; Panettiere et al., 2000; Venturrelli 2003) are also plotted. Dotted curves in (A) and (B) refer to mixing with 0.4% and 2% wt.% NaCl fluid inclusions and MgCl_2 dissolution (1 mol), respectively. Grey crosses and ices correspond, respectively, to mixing with 0.4% and 2% wt.% NaCl fluid inclusions for mixing fractions ranging from 0.001 to 0.005. The solid line refers to mixing of meteoric water (A) or Mg-bicarbonate water (B) with seawater. The vertical grey line represents the water-soluble Cl content in the serpentinites from Northern Apennine (Barnes et al., 2006). Symbols are as in Fig. 2.

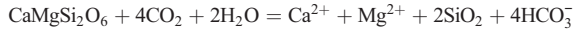


(talc)



(clinochlore)

The Mg-bicarbonate waters issuing from ultramafic rocks fall near this line and cluster between the clinochlore and forsterite points (Fig. 2). Stream waters and springs issuing from sedimentary and basaltic rocks fall between the carbon apex and the line indicated by a C/Mg molar ratio of 4, which describes the dissolution of Ca–Mg-clinopyroxene:



(diopside)

This is consistent with the (Ca)-bicarbonate compositions of these stream waters and springs. It is noteworthy that the Ceno stream waters, shifted toward the C apex of Fig. 2, derive their chemistry from the interaction with Mt. Caio Flysch cropping out widely in the Ceno catchment (samples from UM50 to UM59; see Map1 sheet in the annexes), whereas the Taro source spring waters plot towards the other apexes (lower C) typical of ophiolite minerals (samples from UM41 to UM49; see Map1 sheet in the annexes). The use of the trace elements (e.g., Sr and Rb content; Boschetti, 2003) further highlight the differences between the stream waters of the two rivers and the role of lithology. Nonetheless, mixing and equilibrium with atmosphere make the reaction-path modeling of these samples poorly reliable, so they are unsuitable for the purpose of the present work.

Alkaline waters from ultramafic rocks fall inside the same sub-triangle, mostly along the C–Si side, probably due to the precipitation of magnesium minerals during the evolution of the water composition (Bruni et al., 2002).

4.2. Sodium–chloride relationships

Chlorine and other halogens in serpentinized rocks are inherited from seawater and marine sediments during oceanic metamorphism (e.g. Orberger et al., 1990). They are transferred into serpentinite by adsorption (Anselmi et al., 2000; Sharp and Barnes, 2004), entrapment in fluid inclusions (Scambelluri et al., 2001a,b), and substitution in the structure of low-crystalline iron-hydroxide phases. These latter are composed of the isomorphous and chemically similar iowaite, hibbingite, and Fe–Cl-oxhydroxides (also named green rusts or fougérites; Kohls and Rodda, 1967; Saini-Eidukat et al., 1994; Feder et al., 2005, and references therein). In the Northern Apennine serpentinite rocks, the mean Cl content is ~300 ppm; mean values of 221 and 375 ppm were measured, respectively, in the Erro–Tobbio (Ligurian Western Alps; Scambelluri et al., 2004) and in the central Italy serpentinites (Anselmi et al., 2000), but the water-soluble Cl from serpentinites is estimated to be than 100 ppm (Barnes et al., 2006). As shown in Fig. 2, waters from basalts and ultramafites of the Taro–Ceno Valleys show a trend towards the Cl apex, whereas in Fig. 3 the estimated soluble chlorine in serpentinites agrees with the highest value reported in spring waters from ultramafites (samples from Marini and Ottonello analyzed in 2002). The Cl content of samples UM1 and UM36 is very high (Fig. 3) and is probably due to pollution. In fact, these springs are not far from the A15 highway (UM1) and the Tomarolo Pass road (UM36), where salt mixtures comprising NaCl, MgCl₂·6H₂O, and probably CaCl₂ are widely used for deicing in winter. Alkaline water with a Mg-bicarbonate composition from ultramafites show the highest and lowest Cl contents, respectively. Na-rich Mg-bicarbonate waters from basalts (UM6, UM7; Fig. 3) and ultramafites can be explained by the dissolution of albite in basalts (Beccaluva et al., 1975) and in spilitized EL peridotites (Beccaluva et al., 1984;

Rampone et al., 1995), respectively, whereas the highest content of both Na and Cl in the alkaline water samples UM15 and PR10 (Fig. 3) can be explained by leaching of NaCl fluid inclusions in the serpentinite rocks (0.4–2.0 wt.% NaCl; Scambelluri et al., 2004).

4.3. Boron and B/Cl ratio

Compared with unaltered ultramafic rocks, serpentinites have higher content of both boron and chlorine, and most authors suggest that both elements come from seawater (e.g. Sanford, 1981 and references therein; Bonatti et al., 1984). Despite several studies on these rocks, the behavior of Cl and B in solution during water–rock interaction processes is not well known. Early investigations on fluids associated with serpentinites in the western United States (Barnes and O’Neil, 1969; Barnes et al., 1972) revealed metamorphic waters with high boron levels (up to 28 mM) and B/Cl molar ratios of 0.038–0.13, as well as Mg-bicarbonate and high-pH waters of meteoric origin with variable B/Cl ratios of 0.027–0.42 (median 0.039) and 0.0006–0.017 (median 0.0076), respectively. Bicarbonate waters issuing from ophiolitic rocks in Cyprus have B/Cl ratio in this range (0.0017–0.058, median 0.0019; Neal and Shand, 2002), whereas low boron

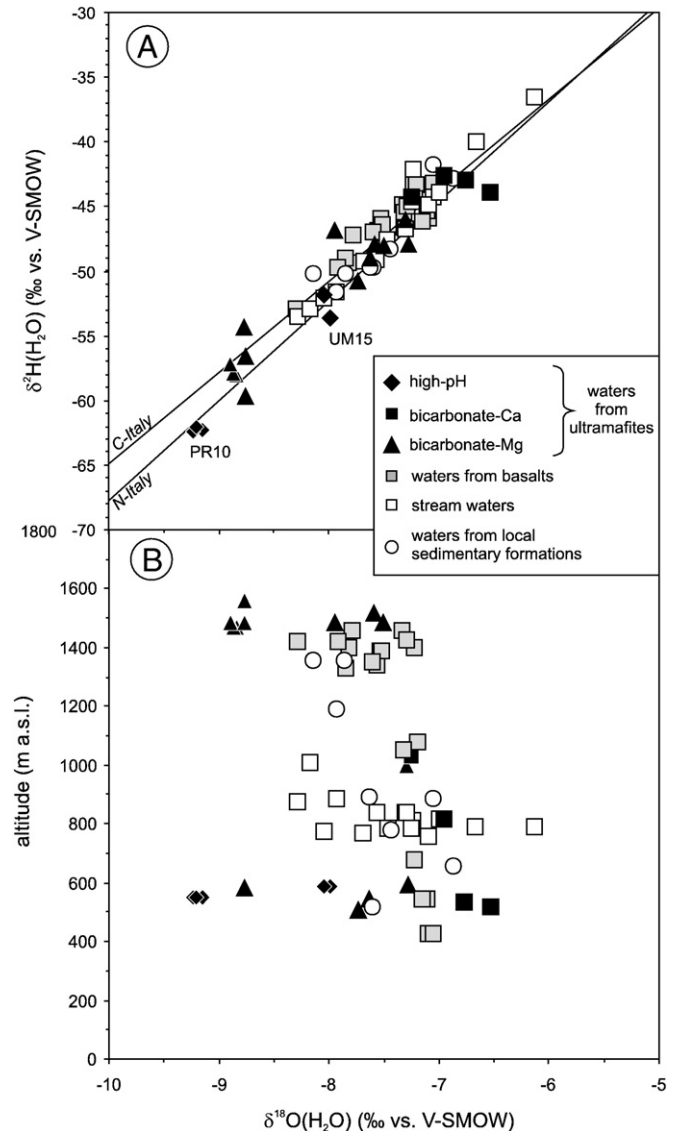


Fig. 4. Plots of (A) $\delta^{18}\text{O}$ vs. $\delta^2\text{H}$ and (B) $\delta^{18}\text{O}$ vs. altitude for waters from the Taro–Ceno Valleys. C-Italy and N-Italy are the meteoric water lines for Central and Northern Italy, respectively (Longinelli and Selmo, 2003). Symbols are as in Fig. 2.

levels were found in the alkaline springs of meteoric origin in Oman, New Caledonia, and ex-Yugoslavia (Barnes et al., 1978).

Among the waters analyzed so far in the Taro–Ceno Valleys, the bicarbonate waters have B/Cl ratios in the range 0.0017–0.22 (median 0.073), whereas the alkaline waters show the highest ratios ever reported (B/Cl=0.34–3.3, median 1.69). The high boron content of up to 13 mg/L of the alkaline springs could be related to metamorphic fluids released during serpentinite subduction; in fact, rocks preferentially lose Cl, and the B/Cl ratio of the released fluids increases with pressure and temperature (Scambelluri et al., 2004). Nonetheless, the alkaline water samples in our study differ significantly from alkaline metamorphic fluids in that they have low salinity, high B/Cl ratios, and meteoric isotope signatures (see below); all these characteristics suggest an origin in the interaction of meteoric water with high-pressure metamorphic serpentinite. This hypothesis is further supported by the agreement in B/Cl ratio between the alkaline samples we study here and the high B/Cl ratio of up to 4 previously reported for the residual high-pressure mineralogy of ultramafites (olivine+orthopyroxene; Scambelluri et al., 2004). In contrast, the Voltri Group's Ca-hydroxide waters have mean values of B=0.14 mg/L and B/Cl=0.03 (Marini and Ottonello 2002), consistent with a contribution of boron and chlorine from fluid inclusions. In fact, assuming fractional contributions of 0.001–0.005 from NaCl fluid inclusions with boron content from 4 to 8 mg/L (Fig. 3a; Scambelluri et al., 2004) results in a B content of 0.004–0.1 mg/L in the solution. These results suggest that the difference between springs from the Voltri Group and Taro–Ceno Valleys is probably related to (i) different evolution of the fluids, and (ii) the different types of host rocks and P–T paths of the Ligurian Western Alps and EL peridotites (e.g. Beccaluva et al., 1984; Scambelluri et al., 2004).

4.4. Isotopic composition of water

A diagram of $\delta^{2}\text{H}$ vs. $\delta^{18}\text{O}$ (Fig. 4A) shows that the waters sampled from the Taro–Ceno Valleys are meteoric in origin, since they are consistent with the meteoric water lines of central and northern Italy (Longinelli and Selmo, 2003). The altitude vs. $\delta^{18}\text{O}(\text{H}_2\text{O})$ (Fig. 4B) summarizes the isotopic effects due to temperature, altitude, and amount of rainfall (e.g. Criss, 1999), all of which help to determine the isotopic composition of the water samples. The tendency is similar for bicarbonate waters from sedimentary, basaltic, and ultramafic forma-

tions, which may provide insight into the recharge areas; alkaline waters, in contrast, probably circulate deeper in the ground.

5. Water–rock interaction model

5.1. Fundamentals

The reaction path model between meteoric water and serpentinite was performed using PHREEQCI 2.12.5 code (Parkhurst and Appelo, 1999) and the Lawrence Livermore National Laboratory thermodynamic database (*lnl.dat*, as known as *thermo.com.V8.R6*) implemented with the equilibrium constants listed in Table 2.

Computations were performed by reaction progress mode (*forward modeling*; Plummer, 1984; Zhu and Anderson, 2002), i.e. (i) adding reacting rock at each step in the simulation, (ii) activating the phase(s) precipitation only when the thermodynamic stability of the mineral paragenesis is well known and consistent with the mineralogy of the area, and (iii) plotting reaction progress on specific activity diagrams. The same thermodynamic database was used with The Geochemist's Workbench 4.0.3 software (Bethke, 2002) to generate Pourbaix and activity diagrams (Figs. 5, 6, 8 and 9). Modeling was performed using an approach based on equilibrium rather than reaction transport, because the data on reaction kinetics and reactive surfaces in these solid phases systems are scarce, particularly with respect to the activation energy of clay and mixed-layer minerals at low temperature and high pH. Moreover, the hydrogeology and the discontinuity of the aquifers in the study area, which are related to the geologic heterogeneity and structural complexity of the Northern Apennine, would make a model based on reaction transport even less credible at this stage.

The modeling in this study was performed on the basis of the following knowledge: (1) primary and secondary mineral assemblages, (2) chemical composition of the minerals involved, (3) physical parameters and chemical composition of the starting fluid, (4) thermodynamic data on pure phases.

5.2. The solid reactant: primary paragenesis

EL peridotites of the Taro–Ceno Valleys (Northern Apennines, Italy) are spinel lherzolites containing olivine (forsterite), orthopyroxene (enstatite), and clinopyroxene (diopside) (Giammetti, 1968 and

Table 2
Thermodynamic data on hydrolysis reactions added to the *lnl.dat* database of the PHREEQCI code (Parkhurst and Appelo, 1999) and *thermo.com.V8.R6.dat* database of The Geochemist's Workbench software (Bethke, 2002)

Mineral	Reaction	log K (T°C)				ΔG_f° (kJ mol ⁻¹)	References
		0	25	60	100		
clinocllore08-daphnite0.2	$\text{Mg}_4\text{Fe}_1\text{Al}_2\text{Si}_3\text{O}_{10}(\text{OH})_8 + 16\text{H}^+ = 2\text{Al}^{3+} + \text{Fe}^{2+} + 12\text{H}_2\text{O} + 4\text{Mg}^{2+} + 3\text{SiO}_2$	73.18	63.84	52.72	42.69	-7863.79	*this work
ferrhydrite 2-line	$\text{Fe}(\text{OH})_3 + 3\text{H}^+ = \text{Fe}^{3+} + 3\text{H}_2\text{O}$	4.84	3.55	-	-	-708.50	Majzlan et al., 2004
ferrhydrite 6-line	$\text{Fe}(\text{OH})_3 + 3\text{H}^+ = \text{Fe}^{3+} + 3\text{H}_2\text{O}$	4.35	3.12	-	-	-711.00	Majzlan et al., 2004
liz0.9-berth0.1	$\text{Mg}_{2.7}\text{Fe}_{0.2}\text{Al}_{0.2}\text{Si}_{1.9}\text{O}_5(\text{OH})_4 + 6.4\text{H}^+ = 0.2\text{Al}^{3+} + 0.2\text{Fe}^{2+} + 5.2\text{H}_2\text{O} + 2.7\text{Mg}^{2+} + 1.9\text{SiO}_2$	31.11	27.86	23.83	20.05	-3998.54	*this work
p-antigorite	$\text{Mg}_3\text{Si}_2\text{O}_5(\text{OH})_4 + 6\text{H}^+ = 3\text{Mg}^{2+} + 2\text{SiO}_2 + 5\text{H}_2\text{O}$	37.67	34.79	31.48	28.46	-	Gunnarsson et al., 2005
Montmorillonite-Fe ²⁺ -Mg	$\text{Fe}_{0.165}\text{Mg}_{0.33}\text{Al}_{1.67}\text{Si}_4\text{O}_{10}(\text{OH})_2 + 6\text{H}^+ = 0.175\text{Fe}^{2+} + 0.35\text{Mg}^{2+} + 1.65\text{Al}^{3+} + 4\text{SiO}_2 + 4\text{H}_2\text{O}$	4.75	3.40	1.39	-1.09	-	Marini and Ottonello, (2002)
Montmorillonite-Fe ³⁺ -Mg	$\text{Fe}_{0.11}\text{Mg}_{0.33}\text{Al}_{1.67}\text{Si}_4\text{O}_{10}(\text{OH})_2 + 6\text{H}^+ = 1.67\text{Al}^{3+} + 0.11\text{Fe}^{3+} + 4\text{H}_2\text{O} + 0.33\text{Mg}^{2+} + 4\text{SiO}_2$	5.14	3.61	1.37	-1.31	-	Marini and Ottonello, (2002)
Saponite-Fe ²⁺	$\text{Fe}_{3.175}\text{Si}_{3.65}\text{Al}_{0.35}\text{O}_{10}(\text{OH})_2 + 7.4\text{H}^+ = 0.35\text{Al}^{3+} + 3.175\text{Fe}^{2+} + 4.7\text{H}_2\text{O} + 3.65\text{SiO}_2$	18.45	16.35	13.19	10.01	-4524.59	Wilson et al., 2006
Saponite-Fe ²⁺ -Mg	$\text{Fe}_{0.165}\text{Mg}_{0.33}\text{Al}_{1.67}\text{Si}_4\text{O}_{10}(\text{OH})_2 + 7.32\text{H}^+ = 0.33\text{Al}^{3+} + 0.165\text{Fe}^{2+} + 4.66\text{H}_2\text{O} + 3\text{Mg}^{2+} + 3.67\text{SiO}_2$	30.37	27.29	23.30	19.21	-	Marini and Ottonello, (2002)
Saponite-Fe ³⁺ -Mg	$\text{Fe}_{0.11}\text{Mg}_{0.33}\text{Al}_{1.67}\text{Si}_4\text{O}_{10}(\text{OH})_2 + 7.32\text{H}^+ = 0.33\text{Al}^{3+} + 0.11\text{Fe}^{3+} + 4.66\text{H}_2\text{O} + 3\text{Mg}^{2+} + 3.67\text{SiO}_2$	30.77	27.50	23.29	19.01	-	Marini and Ottonello, (2002)
Vermiculite-Fe ²⁺ -Mg	$\text{Mg}_{3.05}\text{Fe}_{0.5}\text{Si}_{2.9}\text{Al}_{1.1}\text{O}_{10}(\text{OH})_2 + 10.4\text{H}^+ = 3.05\text{Mg}^{2+} + 2.90\text{SiO}_2 + 1.1\text{Al}^{3+} + 0.5\text{Fe}^{2+} + 6.2\text{H}_2\text{O}$	-	40.87	-	-	-5620.43	this work
Vermiculite-Fe ³⁺ -Mg	$\text{Mg}_{2.675}\text{Fe}_{0.35}\text{Si}_{2.85}\text{Al}_{1.1}\text{O}_{10}(\text{OH})_2 + 10.6\text{H}^+ = 2.675\text{Mg}^{2+} + 2.85\text{SiO}_2 + 1.4\text{Al}^{3+} + 0.35\text{Fe}^{3+} + 6.3\text{H}_2\text{O}$	-	31.71	-	-	-5591.25	this work

The Gibbs free energy of formation (ΔG_f°) of the two theoretical Fe³⁺ (Varadachari et al., 1994) and Fe²⁺ vermiculites were calculated using a previously published method (Vieillard, 2002; and Vieillard, pers. comm.).

*log K values estimated considering an ideal solid solution between the end-members and using data thermodynamic data from *lnl.dat* (clinocllore08-daphnite0.2) and Wilson et al. (2006) (liz0.9-berth0.1).

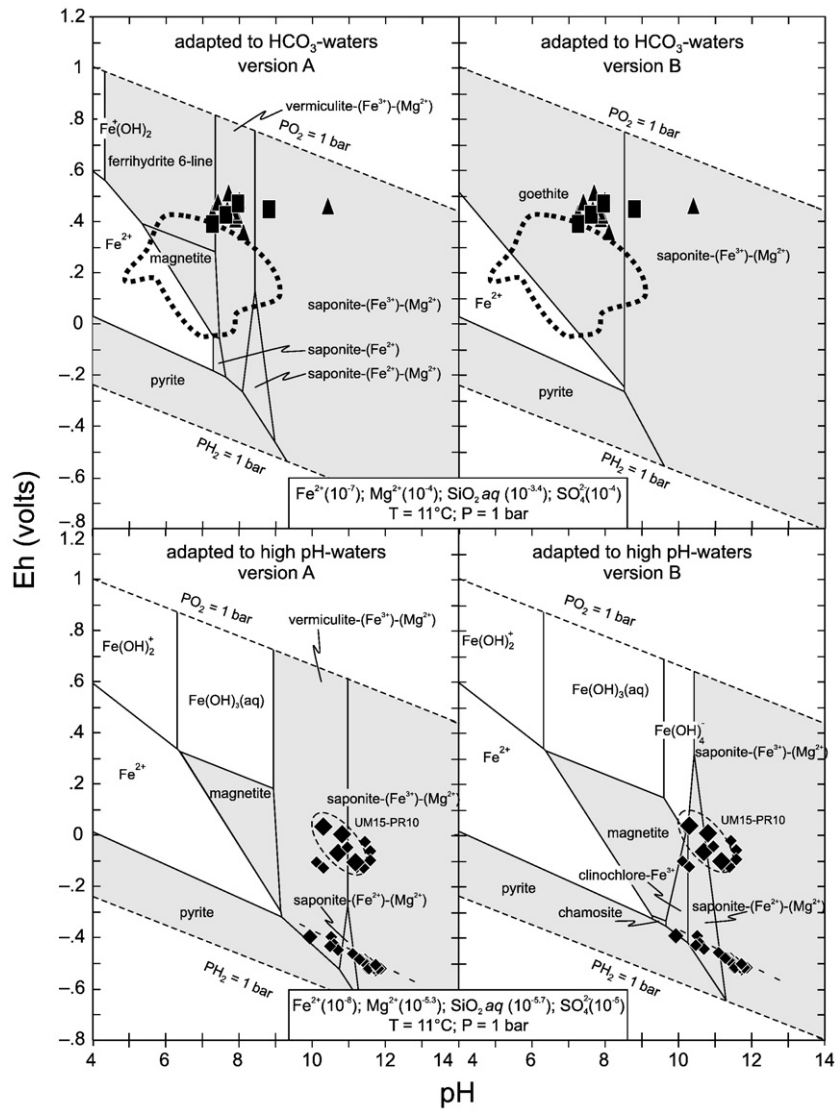


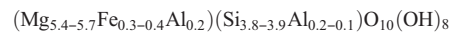
Fig. 5. Eh–pH iron diagram of the spring waters coming from ultramafic rocks of the Taro–Ceno Valleys. Bicarbonate and high-pH waters of the Voltri Group are also represented (dotted area and small black diamonds, respectively). The lowest Eh value of the high-pH waters was calculated using the S(+VI)/S(-II) redox couple (Marini and Ottonello, 2002). The stability field of mineral phases are in grey and those of aqueous species in white. In diagrams A and B, 6-line ferrihydrite-vermiculite and goethite were selected as subaerial solid phases, respectively.

references therein; Venturelli et al., 1997). Accessory phases are plagioclase, picotite ± calcium–sodic amphibole (Venturelli et al., 1997). Before modeling, the crystal chemical formula of the mineral phases was calculated from data from Venturelli et al. (1997); then, depending on the modal composition of the rock (Ernst and Piccardo, 1979) and the composition of the ideal solid solution of the minerals, the resulting stoichiometry of the solid reactant(s) was calculated and inserted in the input file of the PHREEQCI software (Table 3). Thermodynamic data of the primary mineral paragenesis are all well known and are included in the *lnl.dat* thermodynamic database of PHREEQCI.

5.3. The solid reactant: secondary paragenesis

Secondary minerals in the ultramafites of the Taro–Ceno Valleys are serpentine (lizardite and rare chrysotile), smectite minerals (Fe–Mg saponites), and Fe-oxi-hydroxides. Other accessory minerals are chlorite, mixed layer saponite–chlorite (low-charge corrensite), talc, calcite, and dolomite (Beccaluva et al., 1973; Dinelli et al., 1997; Venturelli et al., 1997; Brigatti et al., 1999, 2000). In addition, mixed layer saponite–talc (alietite) and vermiculite–chlorite (high-charge

corrensite) are present (Alietti, 1956; Settembre Blundo et al., 1992; Brigatti and Valdrè, 1996). Except for serpentine, the modal abundance of these phases is unknown. In addition, some of these minerals – particularly interlayer clays – may have different origins (hydrothermal or weathering, allogenic or authigenic) and different stabilities related to kinetics and drainage flow rate. For example, chlorite weathering yields vermiculite-bearing or saponite-bearing interlayers under good- and poor-drainage regimes, respectively (Bonifacio et al., 1997; Środoń, 1999). In addition, the thermodynamic data available for serpentine include information only on chrysotile, which is less abundant than lizardite in the serpentinites of the areas that we studied. According to Venturelli et al. (1997), the lizardite composition in the serpentinites of the Taro valley can be summarized as:



which is similar to 1-T lizardite from the Monte Fico serpentinitized peridotite (Elba Island, Northern Tyrrhenian Sea, Italy; Viti and Mellini, 1997).

Using the thermodynamic data of Wilson et al. (2006) and assuming an ideal solid solution between lizardite and berthierine,

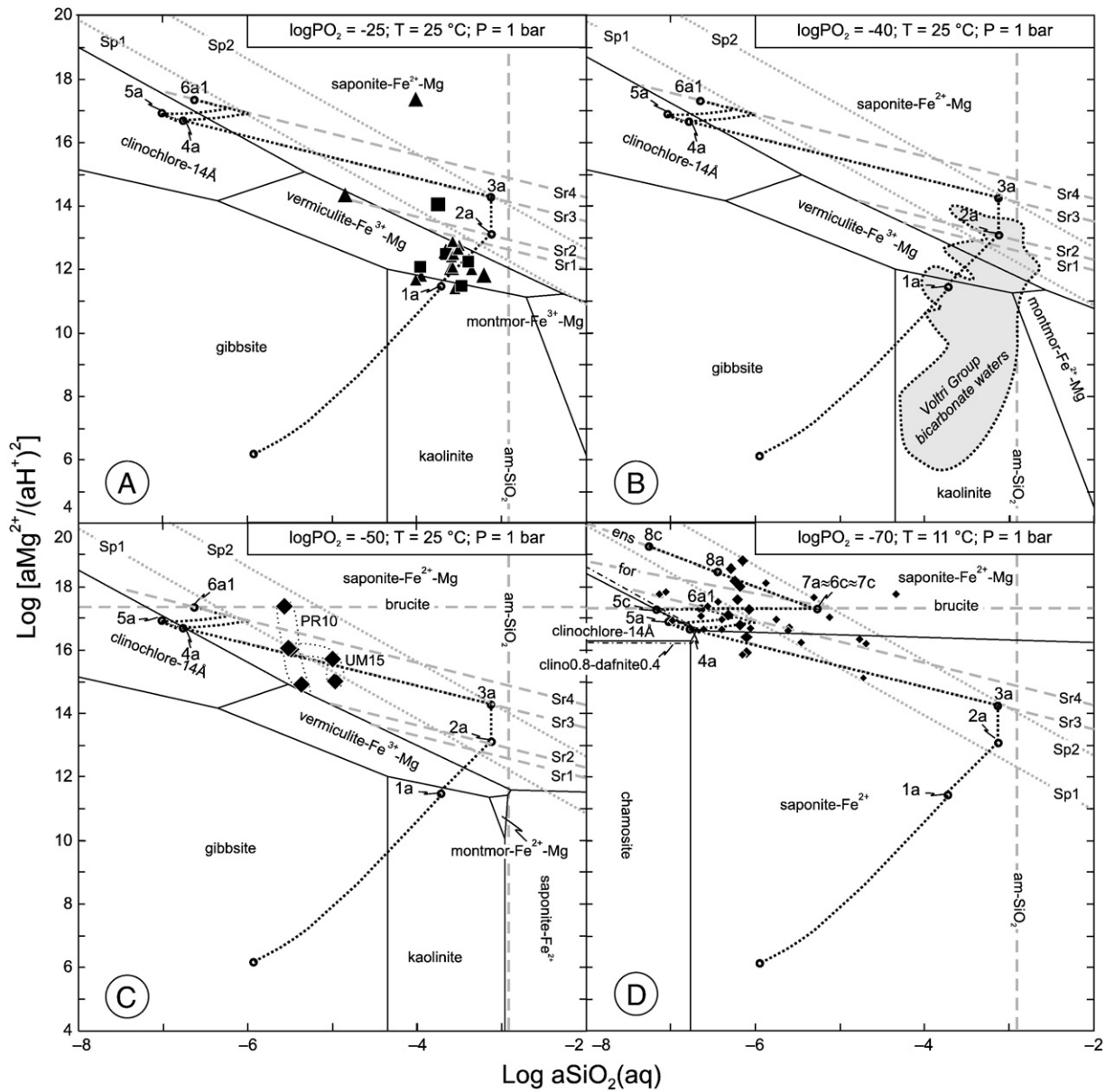


Fig. 6. Activity plot for the $\text{MgO-SiO}_2\text{-Al}_2\text{O}_3\text{-Fe}_2\text{O}_3(\text{FeO})\text{-H}_2\text{O}$ system at different $\log \text{PO}_2$ values. Spring waters issuing from Taro–Ceno Valleys (symbols as in Fig. 2) and Voltri Group ultramafites are shown (grey area, bicarbonate waters; small black diamonds, alkaline waters from Marini and Ottonello, 2002). In plots A, B, and C, the stability field limits of vermiculite (Table 2) correspond to 25 °C; while the amorphous silica (am-SiO_2), brucite, serpentine (Sr1–4 in Table 4), and sepiolite (Sp1–2 in Table 4) phases correspond to 11 °C. The path calculated for interaction between water and ultramafic rock is also shown (dotted line); the number-letter combinations refer to the appearance and disappearance of minerals (see Table 5).

we calculated $\Delta G_f^0 = -3998.54 \text{ kJ/mol}$ for a theoretical (0.9)(lizardite) + (0.1)(berthierine) mineral (Table 2). The $\log K$ value of the stated solid solution was calculated at different temperatures using PHREEQCI after loading the thermodynamic data on the two end-members into the database. The $\log K$ results obtained for Al-lizardite were added to the thermodynamic database of the solid reactant (Table 3), and compared with data from the literature (Table 4).

5.4. Composition of the starting solution, O_2 partial pressure, and minerals included in the model

The weighted average chemical composition of rainwater in Bologna (Panettiere et al., 2000), which is 95 km east of the investigated area, was used as the starting solution in the model. Full chemical data on rainwater of the Taro–Ceno Valleys are unavailable.

Total alkalinity was recalculated for $\log \text{PCO}_2 = -3.5$ bar and $T = 11$ °C, which was the mean temperature of the springs sampled, and for p_e (or E_h) based on chemical data for the redox couple $\text{N}(-\text{III})/\text{N}(+\text{V})$. The values of p_e and E_h obtained were 5.66 and 4.52 ($E_h = 0.25 \text{ V}$), respectively; the former agrees with the median value reported for rainwater in the area (Venturelli et al., 1997). Because data on Al, Fe, and Si in rainwater were lacking, we calculated the concentrations of these elements assuming $\log \text{PCO}_2 = -3.0$ bar and slight supersaturation relative to ferrihydrite-6 line and kaolinite. In this way, a hypothetical composition of water in equilibrium with the local soil was calculated (Table 3) and adopted as the “initial water” for modeling.

Evidence suggests that secondary minerals, particularly Fe-bearing phases, change the chemical composition of the water flowing through the ultramafites of the Taro–Ceno Valleys. According to Neal and Stanger (1983) and Fritz et al. (1992), the production of CH_4 and

Table 3

Starting mineralogy (left side) and fluid composition (right side) used in the modeling

Rock composition				Fluid composition			
Modal % of the minerals in the interacting rock		mol% of the minerals used in the modeling		meteoric water composition		Initial fluid composition used in the modeling	
				Parameter	T (°C)	11	11
48	Olivine	Forsterite	0.43	pH		5.660	5.5
		Fayalite	0.05	pe		14.63	14.821
29	Orthopyroxene	Enstatite	0.26	logP(CO ₂)		-3.5	-3.0
		Ferrosilite	0.03	Molality	Al	-	1.176E-06
10	Al-lizardite	Al-lizardite	0.100		C	1.943E-05	5.876E-05
					Ca	7.660E-05	7.660E-05
8	Clinopyroxene	Diopside	0.06		Cl	3.921E-05	3.921E-05
		Hedernbergite	0.02		Fe	-	5.258E-08
					K	1.151E-05	1.151E-05
					Mg	1.234E-05	1.234E-05
					N	1.308E-04	1.308E-04
5	Spinel	Spinel	0.03		Na	3.523E-05	3.523E-05
		Chromite	0.01		S	3.519E-05	3.519E-05
		Magnetite	0		Si	-	1.176E-06
					Kaolinite	-	5.258E-08*
					Ferrihydrite-Gline	-	5.882E-07*

The modal percentage of the minerals in a serpentinite from Taro–Ceno Valleys (Ernst and Piccardo, 1979) was re-calculated assuming an ideal solid solution between pure extreme phases and taking the modal percentage to be the mass percentage. The latter was used as the solid reactant composition in the water–rock interaction model. Pure solid phases were chosen from the *lml.dat* thermodynamic database of the PHREEQC software. The weighted average chemical composition of the meteoric water from Bologna (Panettiere et al., 2000) was chosen as the initial fluid composition in the modeling, after its equilibration with kaolinite and ferrihydrite (see text for details).

H₂ in the alkaline waters flowing from the ultramafites is related to the consumption of oxygen during the oxidation of iron forming the hematite–magnetite pair. Therefore, the activity of iron and the oxidation state of the water must be defined. The analysis of water samples from ultramafites were plotted in both the Pourbaix and activity diagrams (Figs. 5 and 6), where the calculated activity of Fe²⁺, Mg²⁺, SiO₂, SO₄²⁻ (Pourbaix) and log PO₂ (activity diagrams) were involved. Iron concentration was quite variable in the Taro–Ceno springs, where the average content was 27 µg/L and the content reached a maximum of 200 µg/L, and in the Voltri springs, where the average was 44 µg/L and the maximum was 948 µg/L (Marini and Ottonello, 2002). In both cases, the variations are probably related to the different mineralogies of the soils and the different solubilities of the Fe-rich phases like goethite and ferrihydrite. Iron-bearing saponites and montmorillonites are the prevailing clay minerals in the area investigated, probably because of the ubiquitous presence of iron oxy-hydroxide (Alietti et al., 1976; G. Venturelli, pers. comm.). For this reason, the model considers the involvement of pure Mg-smectite to be negligible.

In the Pourbaix diagram (Fig. 5), the data from bicarbonate waters fall into the ferrihydrite-goethite-vermiculite fields and the data from alkaline waters fall on the boundaries of the vermiculite/saponite and saponite/chlorite. Since ferrihydrite is the first precipitating Fe-phase, it was used rather than goethite in the modeling. The diagram also suggests the transformation of ferrihydrite into magnetite during the change from bicarbonate to alkaline composition, but this process requires a large amount of Fe²⁺ in solution (>2 mM; Hansel et al., 2005), which is unlikely at this stage of the water–rock interaction. Thus, the magnetite participating in the equilibrium is most likely primary in origin.

The modeling and the activity diagrams (Figs. 6 and 9) were calculated using the average value PO₂ = 10⁻²⁶ or 10⁻⁵⁰ bar for bicarbonate and alkaline waters, respectively. These values are compatible with those calculated by Marini and Ottonello (2002) for bicarbonate waters (PO₂ = 10⁻⁴⁰ bar) and for alkaline waters of the Voltri Group (10⁻⁷⁷ bar < PO₂ < 10⁻⁴² bar). The lowest PO₂ value, which was used as a limit in the modeling, was calculated from the S(+VI)/S(-II) redox couple. Moreover, the activity diagrams (Fig. 6) indicate that the data from the bicarbonate waters from the Taro–Ceno Valleys fall between quartz, whose log [SiO₂] = -4.33 is not shown because of the slow precipitation kinetics under the P–T conditions considered

here (Williams et al., 1985), and amorphous silica boundary fields (Fig. 6A); at the same manner, bicarbonate waters with higher SiO₂-activity from the Voltri Group fall on amorphous silica boundary (Fig. 6B). In summary, then, the bicarbonate waters are supersaturated in kaolinite, ferrihydrite, vermiculite, and saponite. Alkaline waters are also supersaturated with saponite (Fig. 6A–C), and they are also equilibrated with primary magnetite and, under extreme conditions, probably pyrite as well.

5.5. Limitations of the model related to kinetics

Model calculations disregard the rates of mineral dissolution and precipitation, which becomes increasingly important as temperature

Table 4Summary of thermodynamic data for the sepiolite (Sp_n) and serpentinite (Sr_n) minerals; phases in italics do not refer to the mentioned hydrolysis reactions

	ΔG_f° (kJ mol ⁻¹)	log K (at 25 °C)	Reference
Sepiolite (Sp _n) – Mg ₄ Si ₆ O ₁₅ (OH) ₂ ·6H ₂ O + 8H ⁺ = 4Mg ²⁺ + 6SiO ₂ + 11H ₂ O	-9254.00	30.04	Gunnarsson et al. (2005)
	-9251.33	30.50 ^a –31.72	Christ et al. (1973)
(Sp1)	-9251.63	30.44	^b thermo.com.V8.R6
	-9248.68	30.97 ^a –31.52	Stoessel (1988)
(Sp2)	-9219.86	36.02 ^a –37.56	Wollast et al. (1968)
Serpentine (Sr _n) – Mg ₃ Si ₂ O ₅ (OH) ₄ + 6H ⁺ = 3Mg ²⁺ + 2SiO ₂ + 5H ₂ O	-2893.24	16.80	Mondésir and Decarreau (1987)
Ni-lizardite	-4110.03	25.44 ^a	Caruso and Chernosky (1979)
Al-lizardite/2	-3398.54	27.86	this work (see text for details)
Al-lizardite	-4040.25	30.56	Wilson et al. (2006)
Mg-lizardite (Sr1)	-4037.02	31.12	^b thermo.com.V8.R6
Mg-crysotile (Sr2)	-4028.24	33.40	Mondésir and Decarreau (1987)
p-antigorite (Sr3)	-5642.39 ^a	34.79	Gunnarsson et al. (2005)
Mg-chrysotile (Sr4)	-4068.09	36.69	Bruni et al. (2002)
Mg-chrysotile/asbestos	-5625.05 ^a	38.88	Pfeifer (1977)
Antigorite	-66128.64	477.19	^b thermo.com.V8.R6

The field boundaries of the underlined phases shown in Fig. 6 correspond to a temperature of 11 °C.

^a In the ΔG_f° column: value calculated using the ΔG_f° data of the elements from *lml.dat* and logK value in the reference; in the LogK column: value calculated using ΔG_f° (mineral) in the reference and ΔG_f° data of the elements from *lml.dat*.

^b Thermodynamic database of Lawrence Livermore National Laboratory, included in PHREEQC and Geochemist's Workbench softwares.

Table 5
(a) Input and (b) output data of the model

Input steps	Gases (log P)		Minerals saturation index															
	CO ₂	O ₂	fer-6line	Kaol	esk	chrom	Fe ³⁺ -Mg-verm	magnet	Fe ²⁺ -Mg-sap	Sr3-serp	†clin-14A	†clino-dafn	Pyr	Sr4-serp	calc	hydrom	Bruc	enst
1a	Start	-3.0	-	0.01	0.01	-	-	-	-	-	-	-	-	-	-	-	-	-
	End	-3.0	-	0.01	0.01	-	-	0.01	-	-	-	-	-	-	-	-	-	-
2a	Start	-3.0	-26	-	0.01	-	-	0.01	0	-	-	-	-	-	-	-	-	-
	End	-3.0	-26	-	0.01	-	-	0.01	0	0.01	-	-	-	-	-	-	-	-
3a	Start	-	-40	-	0.01	-	-	-	0	0.01	-	-	-	-	-	-	-	-
	End	-	-40	-	0.01	-	-	-	0	0.01	-	-	-	-	-	-	-	-
4a	Start	-	-	-	0.01	-	-	-	-	0.01	0.01	-	-	-	-	-	-	-
	End	-	-	-	0.01	-	-	-	-	0.01	0.01	0.01	-	-	-	-	-	-
5a	Start	-	-	-	-	0	-	-	-	0.01	0.01	0.01	-	-	-	-	-	-
	End	-	-	-	-	0	-	-	-	0.01	0.01	0.01	0	-	-	-	-	-
6a1	Start	-	-	-	-	0	-	-	-	0.01	-	-	0	0.01	-	-	-	-
	End	-	-	-	-	0	-	-	-	0.01	-	-	0	0.01	-	-	0.01	-
6a2	Start	-	-	-	-	0	-	-	-	0.01	-	-	0	0.01	0.7	-	-	-
	End	-	-	-	-	0	-	-	-	0.01	-	-	0	0.01	0.7	-	0.01	-
7a	Start	-	-	-	-	0	-	-	-	0.01	-	-	0	-	-	-	0.01	-
	End	-	-	-	-	0	-	-	-	0.01	-	-	0	-	-	-	0.01	0
8a	Start	-	-	-	-	0	-	-	-	0.01	-	-	0	-	-	-	-	0
	End	-	-	-	-	0	-	-	-	0.01	-	-	0	-	-	0.01	-	0
<i>Chlorite dissolution option</i>																		
5c	Start	-	-	-	-	0	-	-	-	0.01	-	-	0	-	-	-	-	-
	End	-	-	-	-	0	-	-	-	0.01	-	-	0	-	-	-	0.01	-
6c	Start	-	-	-	-	0	-	-	-	0.01	-	-	-	-	-	-	0.01	-
	End	-	-	-	-	0	-	-	-	0.01	-	-	-	-	-	-	0.01	0
7c	Start	-	-	-	-	0	-	-	-	0.01	-	-	-	-	-	-	-	0
	End	-	-	-	-	0	-	-	-	0.01	-	-	-	-	-	0.01	-	0
8c	Start	-	-	-	-	0	-	-	-	0.01	-	-	-	-	-	0.01	-	0
	End	-	-	-	-	0	-	-	-	0.01	-	-	-	-	-	0.01	-	0
<i>Output data</i>																		
Output steps		Output data							Moles of dissolved serpentinite									
		pH	Log [SiO ₂]	log [aMg ²⁺ /(aH ⁺) ²]	Log [aCa ²⁺ /(aH ⁺) ²]	tAlk (eq/kg)	SI _{calcite}											
1a	Start	5.45	-5.930	6.05	6.84	4.036.E-06	-5.94											
	End	7.46	-3.741	11.293	10.811	5.524.E-04	-1.98	1.758E-04										
2a	Start	7.46	-3.741	11.293	10.811	5.524.E-04	-1.98											
	End	8.064	-3.136	13.035	12.145	2.324.E-03	-0.64	5.882E-04										
3a	Start	8.064	-3.136	13.035	12.145	2.324.E-03	-0.64											
	End	8.646	-3.140	14.212	13.313	2.431.E-03	-0.06	6.707E-05										
4a	Start	8.646	-3.140	14.212	13.313	2.431.E-03	-0.06											
	End	9.909	-6.803	16.652	16.070	3.432.E-03	1.21	2.377E-03										
5a	Start	9.909	-6.803	16.652	16.070	3.432.E-03	1.21											
	End	10.808	-7.014	16.793	18.533	9.031.E-03	1.99	1.707E-02										
6a1	Start	10.808	-7.014	16.793	18.533	9.031.E-03	1.99											
	End	10.819	-6.626	17.261	18.554	9.148.E-03	1.99	9.600E-05										
6a2	Start	10.657	-6.832	16.607	17.506	6.179.E-03	-											
	End	10.680	-6.626	17.261	17.540	6.347.E-03	-	1.695E-04										
7a	Start	10.819	-6.626	17.261	18.554	9.148.E-03	1.99											
	End	10.819	-5.272	17.261	18.559	9.222.E-03	2.00	1.885E-04										
8a	Start	10.819	-5.272	17.261	18.559	9.222.E-03	2.00											
	End	10.949	-6.464	18.452	18.812	1.064.E-02	2.04	1.092E-03										
<i>Chlorite dissolution option</i>																		
5c	Start	9.857	-6.644	16.547	15.972	3.366.E-03	1.18											
	End	10.202	-7.171	17.262	16.627	3.847.E-03	1.34	3.033E-04										
6c	Start	10.202	-7.171	17.262	16.627	3.847.E-03	1.34											
	End	10.203	-5.272	17.261	16.635	3.860.E-03	1.35	7.100E-05										
7c	Start	10.203	-5.272	17.261	16.635	3.860.E-03	1.35											
	End	10.210	-5.288	17.276	16.649	3.871.E-03	1.35	7.500E-06										
8c	Start	10.210	-5.288	17.276	16.649	3.871.E-03	1.35											
	End	11.300	-7.260	19.248	19.134	3.732.E-03	1.37	2.893E-03										

Abbreviations are as follows: Fer-6line, 6-line ferrihydrite; kaol, kaolinite; verm, vermiculite; magn, magnetite; sap, saponite; serp, serpentine; clin, clinocllore; pyr, pyrite; calc, calcite; hydrom, hydromagnesite; bruc, brucite; enst, enstatite. The chromium decrease during the change in water facies from bicarbonate to alkaline was modeled with supersaturation (precipitation) of eskolaite and thereafter with equilibrium with chromite (Boschetti, 2003).

-: not bound; † chlorite mineral from solution; ‡ chlorite mineral added to the paragenesis.

decreases. The water–rock interaction in the Taro–Ceno basin is complicated by the presence of secondary mixed-layer clay minerals, the origin of which is quite difficult to model because the solid–state transformations and weathering reactions are strictly related to hydrological and climatic conditions, as described above. An equilibrium-based reaction path model is a valuable tool for assessing the

most probable reactions and for defining the product phases that can be used in a kinetics-based model. Since the kinetics of precipitation of Mg-clays at room temperature and pressure are poorly known, relative reaction rate effects in the reaction path model can be mimed by omitting the stabler phase when a metastable mineral is expected to precipitate. Therefore, the precipitation of Mg-Fe³⁺-(Fe²⁺)-

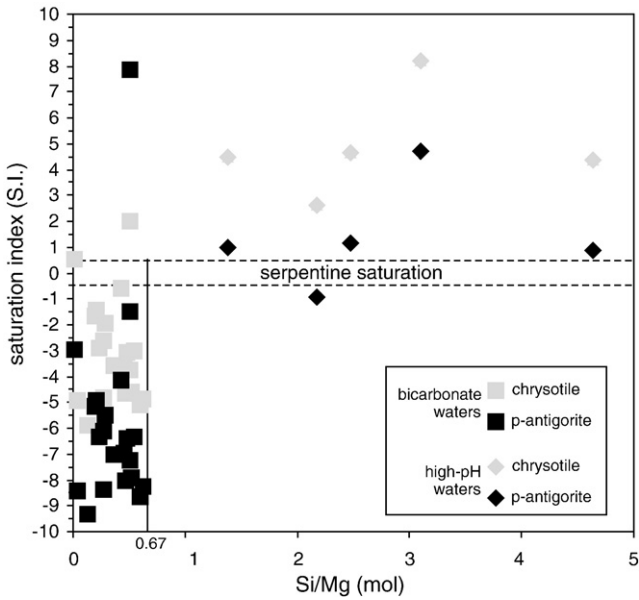


Fig. 7. Saturation indices of chrysotile and p-antigorite (Sr2 and Sr3 thermodynamic data, respectively, in Table 4) for bicarbonate and alkaline waters coming from ultramafic rocks of the Taro–Ceno Valleys as a function of Si/Mg molar ratio. Thermodynamic data on chrysotile and p-antigorite are from the *thermo.com.V8.R6* database and Gunnarsson et al. (2005), respectively.

montmorillonites, vermiculite, and saponites are predicted to occur rather than that of Mg-clays. Moreover, in order to simulate the slow precipitation of calcite in depth, precipitation was not activated at slight supersaturation ($S.I._{calcite} = 0.01$) during the initial stages of the water–rock interaction; in this manner, saturation index of calcite was free to increase in the following steps and in alkaline waters.

6. Discussion of the model results

6.1. Explanation of pre-modeling choices and post-modeling results

The results of the reaction path modeling are reported in Table 5 and shown in Figs. 6 and 9. The reaction paths model the dissolution of a typical local serpentinite (mineralogically constrained as in Table 3) and the sequential precipitation of gibbsite, kaolinite, ferrihydrite, vermiculite, Fe^{2+} – Mg^{2+} -saponite, and a poorly-crystalline serpentine (*p-antigorite* of Gunnarsson et al., 2005). The first step involves the reaction of the “initial water” with serpentinite at constant temperature (11 °C), PO_2 (10^{-26} bar), and PCO_2 ($10^{-3.0}$ bar); this early stage corresponds to bicarbonate groundwater feeding the investigated spring system. At the stage of primary magnetite equilibrium and Fe^{2+} – Mg^{2+} -saponite supersaturation, the model assumes the system to be closed to CO_2 and to have a fixed partial pressure of oxygen ($PO_2 = 10^{-40}$ bar); these conditions represent when water switch from a bicarbonate to an alkaline composition. The calculated amount of interacting serpentinite needed to obtain the alkaline springs of the Taro–Ceno Valleys (mean $PCO_2 = 10^{-7}$ bar) is approximately 0.0203 moles (see Table 5).

Bruni et al. (2002) explained the origin of the alkaline waters of the Voltri Group as the result of the evolution of meteoric bicarbonate water following the precipitation of sepiolite with abundance similar to that of goethite. This might be supported by the observation that sepiolite or smectite precipitate at low temperature from solutions with low Al content when the pH is in the range 7.5–9.5 or >9.5, respectively (Siffert and Wey, 1962; Jones and Galan, 1988), but sepiolites form from the weathering of serpentines in arid climate regions, whereas sepiolites are rare in humid climate regions, where serpentinite changes to Fe-smectite (Singer, 1989; Wrucke, 1996). In the ophiolite rocks of the Northern

Apennine, sepiolite is found only sporadically in veins (Giuseppetti, 1953; Veniale, 1966) and is unknown in the ophiolites of the Taro–Ceno Valleys, whereas it is thought that sepiolite of the Voltri Group precipitated from metasomatic fluids during development of shear zones (Crispini and Capponi, 2002).

As described above, our model explains the transition from bicarbonate water to alkaline water (UM15 and PR10 samples) as the result of low-temperature precipitation of a poor crystalline serpentine with the solubility product of *p-antigorite* (see Sr3 in Table 4 and Fig. 6). The model indicates that the bicarbonate waters of the Voltri Group with the highest $[Mg^{2+}]/[H^+]^2$ activity ratios similarly evolve towards alkaline waters (Fig. 6B). The logK value of the synthetic low temperature serpentine adopted in this model and its

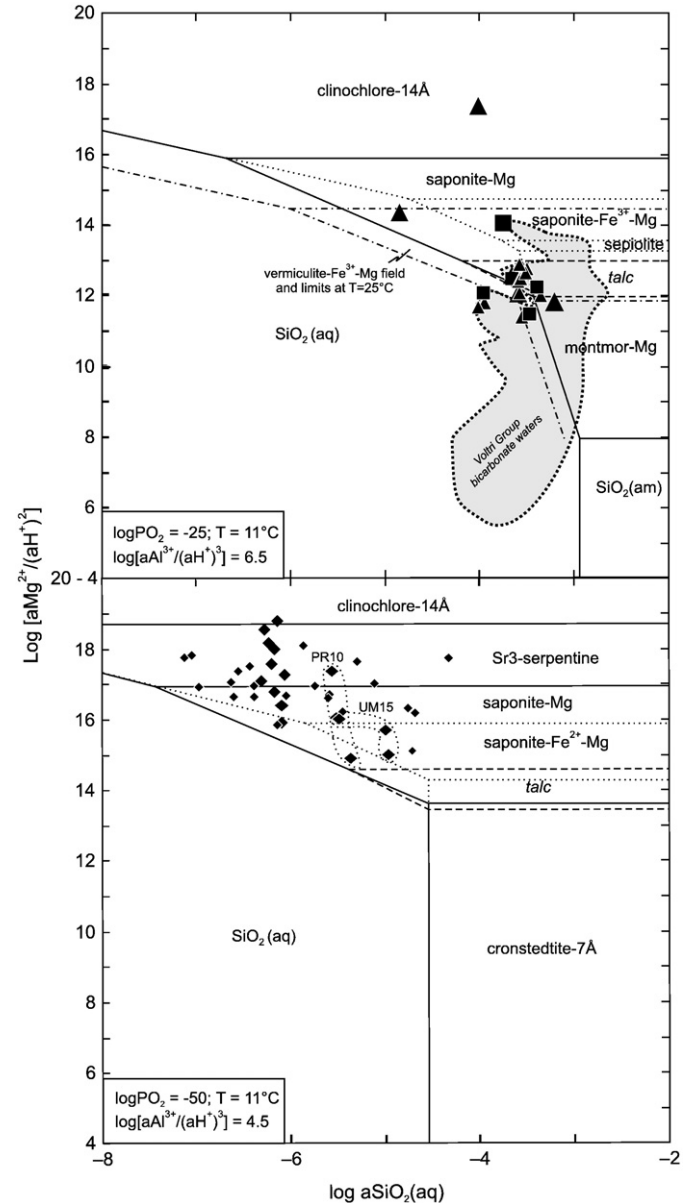


Fig. 8. Activity plot for the MgO–SiO₂–Al₂O₃–Fe₂O₃(FeO)–H₂O system analyzed for SiO₂-phases and aqueous species at different log PO_2 and log $[aAl^{3+}]/(aH^+)^3$ values. Spring waters coming from the Taro–Ceno Valleys (symbols as in Fig. 2) and Voltri Group ultramafites (symbols as in Fig. 5) are shown. The grey area refers to bicarbonate waters from the Voltri Group (Marini and Ottonello, 2002; Bruni et al., 2002). The sepiolite field is very narrow or hidden by saponite-Mg (field limits shown as continuous lines), saponite- Fe^{3+} -Mg (field limits shown as dotted lines), or vermiculite (field limits shown as dotted-dashed lines). The talc stability field and boundaries with saponite-Mg, montmorillonite-Mg, and cronstedite-Mg are shown for comparison (dashed lines).

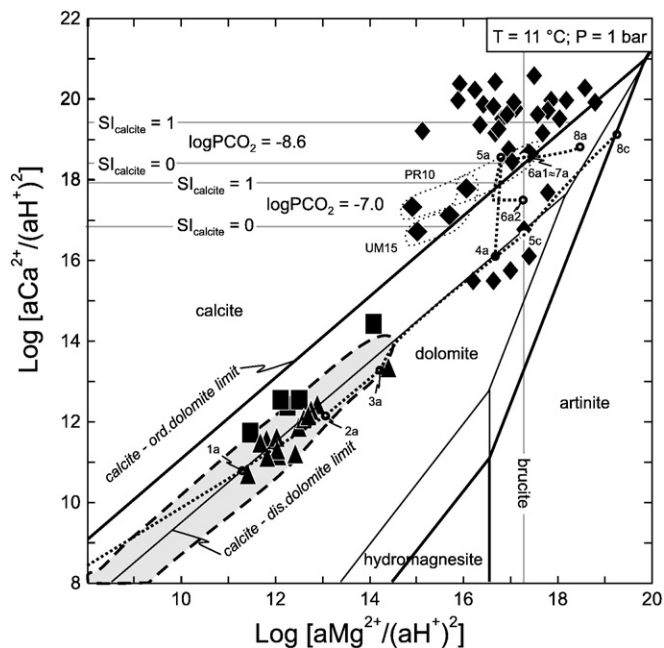


Fig. 9. Activity plot for the MgO–CaO–(CO₂)–H₂O system with phase limits calculated at a temperature of 11 °C. Spring waters coming from the Taro–Ceno Valleys (symbols as in Fig. 2) and Voltri Group ultramafites (symbols as in Fig. 5) are shown. Calculated path for water–ultramafic rock interaction is shown (dotted line), with the number–letter combinations referring to the appearance or disappearance of minerals (see Table 5). The grey area refers to bicarbonate waters from the Voltri Group (Marini and Ottonello, 2002).

relative uncertainty of ± 2 (see Fig. 8 in Gunnarsson et al., 2005) are comparable to the logK variation reported for other low-temperature Mg-serpentines (Table 4), that is within the lines Sr1–4 for serpentine minerals where samples varying from bicarbonate composition to alkaline composition in the ultramafic aquifer are grouped (Fig. 6). Fig. 7 shows a plot of calculated serpentine saturation index as a function of the Si/Mg molar ratio for the water samples from the ultramafites of the Taro–Ceno Valleys. The S.I. and Si/Mg values of pure Mg-serpentine (S.I.=0, Si/Mg=0.67) provide a useful index for separating bicarbonate waters (S.I.<0, Si/Mg<0.67) from alkaline waters (S.I.>0, Si/Mg>0.67), and the distribution of data points is consistent with the idea that bicarbonate waters approach saturation with serpentine until they become supersaturated as alkaline waters.

Based on the Mg vs. SiO₂(aq) activity diagram and specific ratios of log [aAl³⁺/(aH⁺)³], Birsoy (2002) analyzed the behavior of sepiolite during ultramafite weathering. The diagram produces a very narrow stability field for sepiolite (Fig. 8) when it is programmed with suitable conditions for the bicarbonate waters (log PO₂=–25 bar, log [aAl³⁺/(aH⁺)³]=6.5) and the alkaline waters (log PO₂=–50 bar, log [aAl³⁺/(aH⁺)³]=4.5) sampled in the present study. This stability field grows larger when the absence of Mg-smectites and talc is assumed, but this is an unrealistic condition because (i) all these minerals occur in the rocks within the area investigated; and (ii) at high [Mg²⁺]/[H⁺]² activity ratios, the field of sepiolite is smaller than that of subordinate compared to those poorly-crystalline serpentine (p-antigorite) and clinocllore.

Among the alkaline springs of the Voltri Group, the waters with low log [aCa²⁺/(aH⁺)²] values (Fig. 9) show patterns compatible with chlorite interaction (step 5c in Fig. 6D). The alkaline waters whose data fall near the clinocllore–14Å field (Fig. 6D) cannot be explained by sepiolite precipitation, because the sepiolite line does not cross the chlorite fields. Thus, the peculiar composition of some alkaline waters of the Voltri Group is probably due to interactions between water and primary chlorites of the ultramafic rocks (optional step 5c in Table 5c, b). This is supported by the occurrence, sometimes in large amounts, of metasomatic Mg–(Fe)–chlorite (Scambelluri and Rampone, 1999;

Visser and Strating, 2001) in the Ligurian area, where the relative abundance of chlorite can reach 50% in veins in high strain serpentine mylonites of the Erro–Tobbio ultramafites (Scambelluri et al., 2001b). Otherwise, in a chlorite-free primary paragenesis, the solution evolving on the Sr3 serpentine line reaches equilibrium with clinocllore, but probably the latter does not precipitate due to the slow kinetics of precipitation under these conditions. Thus the dissolution of additional reacting rock in the iterative weathering process supplies Mg²⁺ to the solution, thereby favoring the Sr3 to Sr4 poorly crystalline serpentine transformation. In fact, all the PR10 samples and some of the alkaline springs from the Voltri Group show increasing [Mg²⁺]/[H⁺]² activity ratio and low variation in silica activity (Fig. 6D), starting from the invariant triple point 4a (Sr3-serpentine, Fe²⁺–Mg-saponite, clinocllore–14 Å saturation) and extending towards the brucite line. This path can be explained as the result of the transformation of poorly crystalline serpentine from Sr3 to Sr4; the latter is more stable at higher [Mg²⁺]/[H⁺]² activity ratios. Finally, at very low PO₂ values, vermiculite disappears and the stability fields of chlorite and Fe²⁺–Mg-saponite become narrower, whereas those of Fe²⁺–rich phases (e.g. Fe²⁺–saponite) become wider. The data for the alkaline waters with the highest log [aMg²⁺/(aH⁺)²] from the Voltri Group fall near the stability field of peridotite primary minerals like forsterite and enstatite (Fig. 6D); therefore, the last steps of the evolution involve the equilibration of the solution with enstatite (steps 8a and 8c in Table 5a,b).

6.2. Ca-rich alkaline waters

In preliminary modeling of the evolution of the Taro–Ceno spring waters, Boschetti (2003) concluded that meteoric water, initially saturated in Fe³⁺–Mg²⁺–chlorite, Fe³⁺–Mg²⁺–saponite, and pyrite (and/or goethite) and then interacted with the ultramafite mineral assemblage, eventually evolved into the alkaline waters. In the model of Boschetti (2003), chlorite, saponite, and calcite were added

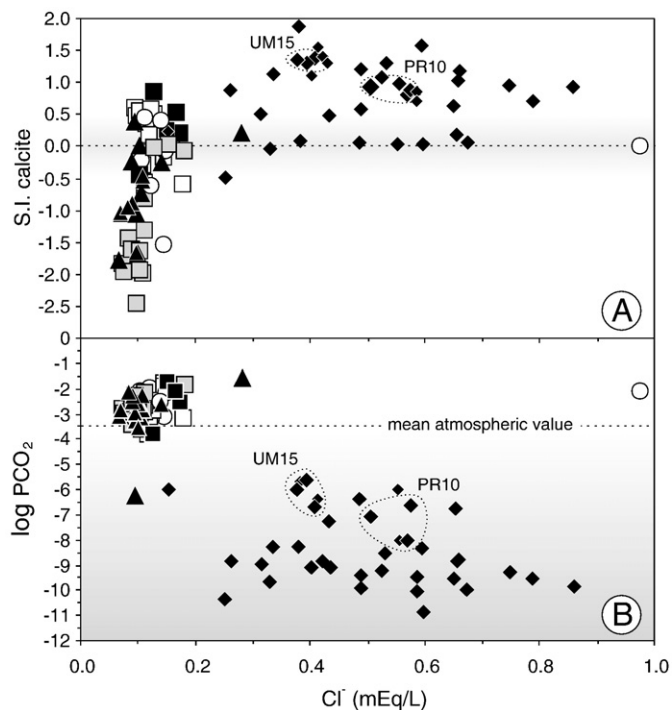


Fig. 10. Plots of (A) calcite saturation indexes and (B) PCO₂ as a function of Cl[–], as calculated by PHREEQCI software for waters from the Taro–Ceno Valleys. Alkaline springs for the Voltri Group are also shown (small black diamonds; Marini and Ottonello, 2002). The grey shading is deeper (A) in the saturation field (SI=0.0±0.5) and (B) where the lowest log PCO₂ value is approached.

to the solution in order to achieve a high $[\text{Ca}^{2+}]/[\text{H}^+]^2$ activity ratio and supersaturation in these phases. However, in light of the work of Clark et al. (1992) and Bruni et al. (2002), we believe that the calcite supersaturation in alkaline waters (Fig. 9 and 10), which in our model is achieved by preventing the precipitation of calcite in the first steps of the reaction path (Table 5a and b), depends on the difference between CO_2 partial pressure at the given depth ($\text{PCO}_2 \leq 10^{-10}$ bar) and at the surface ($\text{PCO}_2 \cong 10^{-3.5}$). Waters rising to the surface are far from equilibrium with the atmosphere, where the PCO_2 is 4×10^6 times greater than the value at depth, thus the water rapidly take up CO_2 , which is promptly converted to CO_3^{2-} because of the high pH. This leads to supersaturation with calcite through the following hydroxylation reaction:



As a result, large amounts of travertine are generated in the Voltri Group (Marini and Ottonello, 2002), and carbonate concretions known as *devil's coins* are formed at Mt. Prinzer in Taro valley. Below the surface, the $S.I._{\text{calcite}}$ of the alkaline waters is expected to be lower than what the model estimates. Under conditions of low carbonate alkalinity, low CO_2 and O_2 partial pressure, and high pH, calcite nucleation may be inhibited and the kinetics of precipitation reduced by the high concentrations of dissolved divalent cations such as Mg^{2+} , Fe^{2+} , and Mn^{2+} (Sumner and Grotzinger, 1996; Davis et al., 2000; Zhang and Dawe, 2000; de Leeuw, 2002). The fact that several alkaline water samples fall within or near the calcite–dolomite equilibrium (Fig. 9) may indicate magnesium calcite or protodolomite nucleation in those extreme subsurface conditions. However, possible interaction between some calcium-rich waters of the Voltri Group and Ca-rich rocks such as ophicarbonates or rodingites cannot be excluded; these rocks are widespread in the Ligurian Apennine serpentinites (Treves and Harper, 1994).

6.3. Sepiolite vs. serpentine nucleation under weathering conditions: constraints on the kinetics and equilibrium-based approaches

The kinetics of precipitation of poorly-crystalline serpentine and sepiolite cannot be compared quantitatively because rate constants are available only for well-ordered crystalline phases (e.g. see Palandri and Kharaka, 2004 for crystalline serpentine). Sepiolite precipitation is often invoked to explain magnesium scavenging from solutions, but the lack of kinetic data for this mineral leads to overly simplistic reaction transport models. These models are forced to use kinetic data for phyllosilicates such as kaolinite or muscovite (e.g. Xu et al., 2001; Bryan, 2005). Moreover, the low-temperature thermodynamic data, even if they are fairly uncertain, show that sepiolite solubility increases with decreasing crystallinity (Table 4; Stoessell, 1988). In fact, crystalline sepiolite requires a long time to reach equilibrium with solution, which imposes a slow control on the water composition (e.g. Stoessell and Hay, 1978). Consequently, in modeling based on reaction transport that simulates freshly precipitated or poorly crystalline sepiolite formation, the $\log K$ value of Wollast et al. (1968) is preferable to the lower values (Suarez and Šimůnek, 1996). This preference agrees with the approach of Mariner (2003) and Jove Colon (2006), who adopt a $\log K$ (25 °C) value for sepiolite of 30.44. It is also similar to that reported by Wollast et al. (1968) and it is six $\log K$ units higher than the value used in *thermo.com.V8.R6* dataset, which is often used (perhaps improperly) to model the supergenic nucleation of sepiolite. In the stability diagram in Fig. 6, where the Sp1 and Sp2 lines represent the stability boundaries of crystalline and poorly-crystalline sepiolite, respectively, the evolution of Taro–Ceno waters from bicarbonate to alkaline (Figs. 6A and C) follows the stability field boundary of the poorly-crystalline serpentine (between Sr2–Sr3 lines) rather than that of the poorly-crystalline sepiolite (Sp2), as postulated in the model. The lines for Sp2, Sr3, and amorphous silica intersect at a common point (Fig. 6D), which is consistent with the nucleation of

sepiolite that typically occurs in solutions that are saturated or supersaturated with amorphous silica and (Mg)-carbonate (e.g. Stoessell and Hay, 1978; Birsoy, 2002). Some bicarbonate waters from the Voltri Group have a silica activity near the amorphous silica boundary (Fig. 6B), but only a few alkaline springs of this group fall on the poorly-crystalline sepiolite boundary line (Sp2; Fig. 6D). Both of these features are inconsistent with the possibility that sepiolite precipitates from supergenic fresh water in the Northern Apennine. Moreover, these two results suggest that values for $\log K(\text{sepiolite}) < 30.44$ (see Table 4) should be used to model the dissolution/precipitation of the well-crystallized phase, that is the most common form for the metasomatic sepiolite found in the investigated area.

7. Conclusions

The waters issuing from ultramafites in the Taro–Ceno Valleys originate from low-temperature interactions between meteoric water and serpentinite rocks. In this report, the water–rock interaction has been modeled using reaction paths in progress mode. During their early interaction with soil and rock minerals, bicarbonate waters supersaturated in kaolinite, ferrihydrite, vermiculite, and Fe^{2+} – Mg^{2+} –saponite, where the origin of the secondary iron saponite as Fe^{2+} -bearing smectite agrees with the hypothesis of Güven (1988). Then, while remaining supersaturated with saponite, the bicarbonate waters evolve into an alkaline facies when poorly-crystalline serpentine precipitates. During rock weathering, the Al-bearing crystalline serpentine of oceanic origin probably promotes nucleation of the low-temperature serpentine amorphous phase and supplies Al^{3+} to the solution for saponite precipitation. This interpretation is consistent with the existence of Al-poor supergenic serpentine (Neal and Stanger, 1985) and the partially meteoric OH-isotopic imprint observed in other ultramafic systems.

Difficulties and complexities in the modeling arise from uncertainties in the primary mineralogy of some local ophiolites and from the presence of different lithotypes (rodingites, ophicarbonates, gabbros), which can significantly affect the composition of water samples. This can be seen in the example of the Ca–OH springs issuing from the Voltri Group (PO_2 and PCO_2 of 10^{-70} and 10^{-10} bar, respectively; Bruni et al., 2002; Marini and Ottonello, 2002). These springs appear to be more evolved than the Taro–Ceno alkaline waters, as a result of their particularly long interactions with serpentinites until equilibrium with enstatite is reached, or with chlorite-bearing serpentinite. The use of an updated thermodynamic database in our model avoided problems due to mineralogical heterogeneity in the mixed-layer clays associated with ophiolitic rocks; this database accurately reflected the chemical composition of the single phases. Using this model, the vermiculite–chlorite and saponite–chlorite associations seen in the activity diagrams simulate, respectively, the presence of high and low charge co-rents observed in the field. The accuracy of our model can be tested by comparing estimates of chlorine composition resulting from our model and from experimental methods. The mean Cl concentration of the bicarbonate water is 4.1 ± 1.6 mg/L; taking into account a Cl concentration of ~ 2 mg/L in rainwater in the area (c.f. Panettiere et al., 2000; Venturelli, 2003), 2 mg/L of Cl in spring water are estimated to come from serpentinite. This value agrees with the model, which predicts that the switch from bicarbonate water to alkaline water requires the congruent dissolution of 0.0203 mol of serpentinite, containing 100 ppm of soluble Cl, thereby yielding water containing 2 ppm of Cl.

In addition, we think that weathering of the accessory albite plagioclase is responsible for Na enrichment of the waters, whereas Cl enrichment in the alkaline waters is predicted to result from the leaching of NaCl fluid inclusions. Moreover, the Taro–Ceno alkaline springs show the highest B/Cl ratios, comparable with those of the host metamorphic minerals (Scambelluri et al., 2004). In contrast, the lower boron content and B/Cl ratio of the alkaline springs of the Voltri

Group are unexpected features, and probably reflect water–rock interactions over a longer time period than in the Tarò–Ceno Valleys. The boron content in the Northern Apennine alkaline springs may be controlled by several factors, such as (i) the different histories of Voltri Group and EL ultramafites; (ii) the probable contribution of boron from NaCl fluid inclusions; (iii) the sinking of boron by travertine precipitation (Hobbs and Reardon, 1999), brucite (Rhoades et al., 1970) and smectite; and (iv) decreases in boron release from minerals due to increases in pH (Su and Suarez, 2004).

Acknowledgements

This research was carried out with the financial support from the “Young Researchers Project” (2001–2002) of the Italian Ministry of Universities, Scientific Research, and Technology (MURST). We thank Gianni Cortecchi (Institute of Geosciences and Earth Resources, I.G.G.-C.N.R., Pisa, Italy) and Giampiero Venturelli (Earth Sciences Department, University of Parma, Italy) for useful suggestions and critical review of the manuscript. The authors are grateful to Enrico Dinelli (Interdepartment Research Centre for Environmental Sciences, Alma Mater Studiorum, University of Bologna, Ravenna, Italy) for granting permission to use the Geochemist’s Workbench software. The constructive reviews of the Editor J. Fein and of two anonymous Referees have significantly improved the manuscript.

Appendix A. Supplementary data

Supplementary data associated with this article can be found, in the online version, at doi:10.1016/j.chemgeo.2008.08.017.

References

- Abbate, E., Bortolotti, V., Passerini, P., 1980. Olistostromes and olistoliths. In: Sestini, G. (Ed.), Development of the Northern Apennines geosyncline. *Sedimentary Geology*, 4, pp. 521–558.
- Alietti, A., 1956. Il minerale a strati misti saponite-talco di monte Chiaro (val di Tarò, Appen. Emil.). *Rendiconti dell’Accademia Nazionale dei Lincei* 21, 201–207.
- Alietti, A., De Angelis, G., Montanari, G., Sgarlata, F., Tirelli, G., 1976. Il ferro nelle argille appenniniche. *Periodico di Mineralogia* 45, 51–64.
- Anselmi, B., Mellini, M., Viti, C., 2000. Chlorine in the Elba, Monti Livornesi, and Murlo serpentines. Evidence for sea–water interaction. *European Journal of Mineralogy* 12, 137–146.
- Apha-Awwa-Wef, 1995. Standard Methods for the Examination of Water and Wastewater, 19th Edition. American Public Health Association, American Water Works Association, Water Environment Federation.
- Barnes, I., LaMarche Jr., V.C., Himmelberg, G.R., 1967. Geochemical evidence of present-day serpentinization. *Science* 156, 830–832.
- Barnes, I., O’Neil, J.R., 1969. The relationship between fluids in some fresh alpine-type ultramafics and possible modern serpentinization, Western United States. *Geological Society of America Bulletin* 80, 1947–1960.
- Barnes, I., O’Neil, J.R., Trescases, J.J., 1978. Present day serpentinization in New Caledonia, Oman and Yugoslavia. *Geochimica et Cosmochimica Acta* 42, 144–145.
- Barnes, I., Rapp, J.B., O’Neil, J.R., Sheppard, R.A., Gude III, A.J., 1972. Metamorphic assemblages and the direction of flow of metamorphic fluids in four instances of serpentinization. *Contributions to Mineralogy and Petrology* 35, 263–276.
- Barnes, J.D., Selverstone, J., Sharp, Z.D., 2006. Chlorine isotope chemistry of serpentinites from Elba, Italy, as an indicator of fluid source and subsequent tectonic history. *Geochemistry, Geophysics, Geosystems* 7. doi:10.1029/2006GC001296.
- Beccaluva, L., Emiliani, F., Venturelli, G., Zerbi, M., 1973. Ca, Fe, Mg, Mn, Cr, Ni, Co distribution in some ultramafic rocks outcropping in the Northern Apennines with some geological remarks. *Ateneo Parmense, Acta Naturalia* 9, 69–98.
- Beccaluva, L., Macciotta, G., Piccardo, G.B., Zeda, O., 1984. Petrology of lherzolitic rocks from the Northern Apennine ophiolites. *Lithos* 17, 299–316.
- Beccaluva, L., Venturelli, G., Zanucchi, G., 1975. Dati geologici e geochimici sui basalti di associazione ofiolitica dell’Appennino ligure-emiliano. *Ateneo Parmense, Acta Naturalia* 11, 789–802.
- Bethke, C.M., 2002. The Geochemist’s Workbench. A User’s Guide to Rxn, Act2, Tact, React, and Gtplot Release 4.0. Hydrogeology Program, University of Illinois, Urbana, IL 236 pp.
- Birsoy, R., 2002. Formation of sepiolite–palygorskite and related minerals from solution. *Clays and Clay Minerals* 50, 736–745.
- Bonatti, E., Lawrence, J.R., Morandi, N., 1984. Serpentinization of oceanic peridotites: temperature dependence of mineralogy and boron content. *Earth and Planetary Science Letters* 70, 88–94.
- Bonifacio, E., Zanini, E., Boero, V., Franchini-Angela, M., 1997. Pedogenesis in a soil catena on serpentinite in north-western Italy. *Geoderma* 75, 33–51.
- Boschetti, T., 2003. Studio geochimico e geochimico-isotopico di acque a composizione estrema e termali dell’Appennino Settentrionale. Ph. D. Thesis, Parma Univ.
- Brigatti, M.F., Franchini, G., Lugli, C., Medici, L., Poppi, L., Turci, E., 2000. Interactions between aqueous chromium solutions and layer silicates. *Applied Geochemistry* 15, 1307–1316.
- Brigatti, M.F., Lugli, C., Poppi, L., Venturelli, G., 1999. Iron-rich saponite: dissolution reactions and Cr uptake. *Clay Minerals* 34, 637–645.
- Brigatti, M.F., Valdrè, G., 1996. Mixed-layer chlorite/smectite (corrensite) in ophiolitic rock alteration products. *Neues Jahrbuch fuer Mineralogie, Monatshefte* 1, 37–47.
- Bruni, J., Canepa, M., Chiodini, G., Cioni, R., Cipolli, F., Longinelli, A., Marini, L., Ottonello, G., Vetuschi Zuccolini, M., 2002. Irreversible water–rock mass transfer accompanying the generation of the neutral, Mg–HCO₃ and high-pH, Ca–OH spring waters of the Genova province, Italy. *Applied Geochemistry* 17, 455–474.
- Bryan, C.R., 2005. Drift-Scale THC Seepage Model. MDL-NBS-HS-000001 REV 04, Yucca Mountain Project, Las Vegas, Nevada (US).
- Caruso, L.J., Chernosky, J.V., 1979. The stability of lizardite. *Canadian Mineralogist* 17, 757–769.
- Clark, I.D., Fontes, J.C., Fritz, P., 1992. Stable isotope disequilibria in travertine from high pH waters: Laboratory investigations and field observations from Oman. *Geochimica et Cosmochimica Acta* 56, 2041–2050.
- Cortesogno, L., 1980. Il metamorfismo giurassico nelle ofioliti dell’Appennino Settentrionale: due distinti cicli metamorfici in ambiente oceanico. *Ofioliti* 5, 5–18.
- Christ, C.L., Hostetler, P.B., Siebert, R.M., 1973. Studies in the system MgO–SiO₂–CO₂–H₂O: III. *American Journal of Science* 273, 65–83.
- Cortesogno, L., Lucchetti, G., 1982. Il metamorfismo oceanico nei gabbri ofiolitici dell’Appennino Ligure: Aspetti mineralogici e petrogenetici. *Rendiconti della Società Mineralogica Italiana* 38, 561–579.
- Crispini, L., Capponi, G., 2002. Control of metasomatic alteration on the development of shear zone in ultramafic rocks: a case study from the Voltri Massif (Ligurian Alps). Architettura interna e cinematica delle zone di taglio. Gruppo Italiano di Geologia Strutturale – Riunione Annuale 2002. Pisa, Italy 11–12 giugno 2002, XIV–XV.
- Criss, R.E., 1999. Principles of stable isotope distribution. Oxford University Press, New York.
- Davis, K.J., Dove, P.M., De Yoreo, J.J., 2000. The role of Mg²⁺ as an impurity in calcite growth. *Science* 290, 1134–1137.
- de Leeuw, N.H., 2002. Molecular dynamics simulations of the growth inhibiting effect of Fe²⁺, Mg²⁺, Cd²⁺, and Sr²⁺ on calcite crystal growth. *Journal of Physical Chemistry B* 106, 5241–5249.
- De Nardo, M.T., Segadelli, S., Vescovi, P., 2007. Studio pilota per la caratterizzazione geologica delle sorgenti nella zona del M. Nero (alta Val Ceno e alta Val Nure – province di Parma e Piacenza). *Il Geologo dell’Emilia-Romagna* 25, Nuova Serie, pp. 5–21.
- Di Giulio, A., Geddo, G., 1990. Studio petrografico delle Arenarie di Casanova (alta val Trebbia, Appennino settentrionale). *Atti Ticinesi di Scienze della Terra* 33, 243–254.
- Dinelli, E., Lombini, A., Simoni, A., Ferrari, C., 1997. Heavy metals in serpentinite soils of selected outcrops of Piacenza and Parma provinces (Northern Apennines, Italy). *Mineralogica et Petrographica Acta* 40, 241–255.
- Epstein, S., Mayeda, T., 1953. Variation of ¹⁸O content of waters from natural sources. *Geochimica et Cosmochimica Acta* 4, 213–224.
- Ernst, W.G., Piccardo, G.B., 1979. Petrogenesis of some Ligurian peridotites. I. Mineral and bulk-rock chemistry. *Geochimica et Cosmochimica Acta* 43, 219–237.
- Feder, F., Trolard, F., Klingelhofer, G., Bourrié, G., 2005. In situ Mössbauer spectroscopy: evidence for green rust (fougerite) in a geyser and its mineralogical transformations with time and depth. *Geochimica et Cosmochimica Acta* 69, 4463–4483.
- Fritz, P., Clark, I.D., Fontes, J.C., Whitticar, M.J., Faber, E., 1992. Deuterium and ¹³C evidence for low temperature production of hydrogen and methane in a highly alkaline groundwater environment in Oman. In: Kharaka, T.K., Maest, A.S. (Eds.), Proceedings of the 7th International Symposium on Water–Rock Interaction. Balkema, Rotterdam, pp. 793–796.
- Giammetti, F., 1968. Le ofioliti di Roccaprebalza, Costa della Guardia e Groppo di Gorro (Appennino Parmense). *Ateneo Parmense, Acta Naturalia* 4, 107–142.
- Giuseppetti, G., 1953. Rocce e minerali della formazione ofiolitica di Volpedo. *Rendiconti della Società Mineralogica Italiana* 9, 85–134.
- Gran, G., 1952. Determination of equivalence point in the potentiometric titration. *Analyst* 77, 661–671.
- Gunnarsson, I., Arnorsson, S., Jakobsson, S., 2005. Precipitation of poorly crystalline antigorite under hydrothermal conditions. *Geochimica et Cosmochimica Acta* 69, 2813–2828.
- Güven, N., 1988. Smetites. In: Bailey, S.W. (Ed.), Reviews in Mineralogy 19. Hydrrous phyllosilicates (exclusive of micas). Mineralogical Society of America, Michigan. Book Crafters, Inc., 497–559.
- Hansel, C.M., Benner, S.G., Fendorf, S., 2005. Competing Fe(II)-induced mineralization pathways of ferrihydrite. *Environmental Science and Technology* 39, 7147–7153.
- Hobbs, M.Y., Reardon, E.J., 1999. Effect of pH on boron co-precipitation by calcite: further evidence for non-equilibrium partitioning of trace elements. *Geochimica et Cosmochimica Acta* 63, 1013–1021.
- Jones, B.F., Galan, E., 1988. Sepiolite and palygorskite. In: Bailey S.W. (Ed.), Hydrrous Phyllosilicates (exclusive of Micas). Reviews in Mineralogy, vol. 19. Mineralogical Society of America, Michigan. Book Crafters, Inc. 631–674.
- Jove Colon, C.F., 2006. Technical work plan for: Thermodynamic database for chemical modelling. TWP-MGR-PA-000039 REV 01, Yucca Mountain Project, Las Vegas, Nevada (US).
- Kohls, D.W., Rodda Jr., J.L., 1967. Iowaite, a new hydrous magnesium hydroxide–ferric oxychloride from the Precambrian of Iowa. *American Mineralogist* 52, 1261–1271.
- Kyser, T.K., O’Hanley, D.S., Wicks, F.J., 1999. The origin of fluids associated with serpentinization processes: evidence from stable-isotope compositions. *Canadian Mineralogist* 37, 223–237.
- Lapham, D.M., 1961. New data on deweylite. *American Mineralogist* 46, 168–188.
- Lee, B.D., Sears, S.K., Graham, R.C., Amrhein, C., Vali, H., 2003. Secondary mineral genesis from chlorite and serpentine in an ultramafic soil toposequence. *Soil Science Society of America Journal* 67, 1309–1317.

- Longinelli, A., Selmo, E., 2003. Isotopic composition of precipitation in Italy: a first overall map. *Journal of Hydrology* 270, 75–88.
- Majzlan, J., Navrotsky, A., Schwertmann, U., 2004. Thermodynamics of iron oxides: Part III. Enthalpies of formation and stability of ferrihydrite ($\sim\text{Fe}(\text{OH})_3$), schwertmannite ($\sim\text{Fe}(\text{OH})_3/4(\text{SO}_4)_{1/8}$), and $\varepsilon\text{-Fe}_2\text{O}_3$. *Geochimica et Cosmochimica Acta* 68, 1049–1059.
- Mariner, P., 2003. In-Drift Precipitates/Salts Model. ANL-EBS-MD-000045 REV 01, Yucca Mountain Project, Las Vegas, Nevada (US).
- Marini, L., Ottonello, G., 2002. Atlante degli acquiferi della Liguria. Volume III: Le acque dei complessi ofiolitici (bacini: Arrestra, Branega, Cassinelle, Cerusa, Erro, Gorzente, Leira, Lemme, Lerone, Orba, Piota, Polcevera, Rumarò, Sansobbia, Stura, Teiro, Varenna, Visone). Pacini, Pisa.
- Mellini, L., Zanazzi, P.F., 1987. Crystal structures of lizardite-I T and lizardite-2H1 from Coli, Italy. *American Mineralogist* 72, 943–948.
- Mezzadri, G., 1964. Petrografia delle arenarie di Ostia. *Rendiconti Società Mineralogica Italiana* 20, 192–228.
- Mondesir, H., Decarreau, A., 1987. Synthèse entre 25 et 200 °C de lizardites Ni–Mg. Mesure des coefficients de partage solide-solution aqueuse pour le couple Ni–Mg dans des lizardites. *Bulletin de Mineralogie* 110, 409–426.
- Neal, C., Shand, P., 2002. Spring and surface water quality of the Cyprus ophiolites. *Hydrology and Earth System Sciences* 6, 797–817.
- Neal, C., Stanger, G., 1983. Hydrogen generation from mantle source rocks in Oman. *Earth and Planetary Science Letters* 66, 315–320.
- Neal, C., Stanger, G., 1984. Calcium and magnesium hydroxide precipitation from alkaline groundwaters in Oman, and their significance to the process of serpentinization. *Mineralogical Magazine* 48, 237–241.
- Neal, C., Stanger, G., 1985. Past and present serpentinization of ultramafic rocks; an example from Semail ophiolite nappe of Northern Oman. In: Drever, J.L. (Ed.), *The Chemistry of Weathering*. D. Reidel Publishing Company, pp. 249–275.
- Nesbitt, H.W., Bricker, O.P., 1978. Low temperature alteration processes affecting ultramafic bodies. *Geochimica et Cosmochimica Acta* 42, 403–409.
- Nordstrom, D.K., 1977. Thermodynamic redox equilibria of Zobell's solution. *Geochimica et Cosmochimica Acta* 41, 1835–1841.
- O'Hanley, D.S., 1996. Serpentinites: records of tectonic and petrological history. Oxford University Press.
- Orberger, B., Friedrich, G., Woermann, E., 1990. The distribution of halogens and carbon in Pge-bearing ultramafics of the Acoje Ophiolite Block, Zambales, Philippines. *Journal of Geochemical Exploration* 37, 147–169.
- Ottonello, G., Joron, J.L., Piccardo, G.B., 1984. Rare Earth and 3d transition elements geochemistry of peridotitic rocks: II. Ligurian peridotites and associated basalts. *Journal of Petrology* 25, 373–393.
- Palandri, J.L., Kharaka, Y.K., 2004. A compilation of rate parameters of water-mineral interaction kinetics for application to geochemical modeling. Open File Report 2004-1068. U.S. Geological Survey.
- Panettiere, P., Cortecchi, G., Dinelli, E., Bencini, A., Guidi, M., 2000. Chemistry and sulfur isotopic composition of precipitation at Bologna, Italy. *Applied Geochemistry* 15, 1455–1467.
- Parkhurst, D.L., Appelo, C.A.J., 1999. User's guide to PHREEQC (version 2) — a computer program for speciation, batch-reaction, one-dimensional transport and inverse geochemical calculation. US Department of the Interior. US Geological Survey, Washington DC.
- Pfeifer, H.R., 1977. A model for fluids in metamorphosed ultramafic rocks. Observations at surface and subsurface conditions (high pH spring waters). *Schweizerische Mineralogische und Petrographische Mitteilungen* 57, 361–396.
- Plummer, L.N., 1984. Geochemical modeling: A comparison of forward and inverse methods. In: Hitchon, B., Wallick, E.I. (Eds.), *Proceedings First Canadian/American Conference on Hydrogeology-Practical Applications of Ground Water Geochemistry Banff, Alberta, Canada* — Worthington, Ohio. National Water Well Association, pp. 149–177.
- Rampone, E., Hofmann, A.W., Piccardo, G.B., Vannucci, R., Bottazzi, P., Ottolini, L., 1995. Petrology, mineral and isotope geochemistry of the External Ligurides peridotites (Northern Apennines, Italy). *Journal of Petrology* 36, 81–105.
- Rampone, E., Hofmann, A.W., Piccardo, G.B., Vannucci, R., Bottazzi, P., Ottolini, L., 1996. Trace element and isotope geochemistry of depleted peridotites from an N-MORB type ophiolite (Internal Liguride, N. Italy). *Contributions to Mineralogy and Petrology* 123, 61–76.
- Rhoades, J.D., Ingvalson, R.D., Hatcher, J.T., 1970. Adsorption of boron by ferromagnesian minerals and magnesium hydroxide. *Soil Science Society of America Journal* 34, 938–941.
- Saini-Eidukat, B., Kucha, H., Keppler, H., 1994. Hibbingite, $\gamma\text{-Fe}_2(\text{OH})_3\text{Cl}$, a new mineral from the Duluth Complex, Minnesota, with implications for the oxidation of Fe-bearing compounds and the transport of metals. *American Mineralogist* 79, 555–561.
- Sanford, R.F., 1981. Mineralogical and chemical effects of hydration reactions and applications to serpentinization. *American Mineralogist* 66, 290–297.
- Scambelluri, M., Müntener, O., Ottolini, L., Pettke, T.T., Vannucci, R., 2004. The fate of B, Cl and Li in the subducted oceanic mantle and in the antigorite breakdown fluids. *Earth and Planetary Science Letters* 222, 217–234.
- Scambelluri, M., Rampone, E., 1999. Mg-metasomatism of oceanic gabbros and its control on Ti-clinohumite formation during eclogitization. *Contributions to Mineralogy and Petrology* 135, 1–17.
- Scambelluri, M., Bottazzi, P., Trommsdorff, V., Vannucci, R., Hermann, J., Gómez-Pugnaire, M.T., López-Sánchez Vizcaino, V., 2001a. Incompatible element-rich fluids released by antigorite breakdown in deeply subducted mantle. *Earth and Planetary Science Letters* 192, 457–470.
- Scambelluri, M., Rampone, E., Piccardo, G., 2001b. Fluid and element cycling in subducted serpentinite: a trace-element study of the Erro–Tobbio high-pressure ultramafites (Western Alps, NW Italy). *Journal of Petrology* 42, 55–67.
- Segadelli, S., 2006. La geologia nel paesaggio: le rupi ofiolitiche in Val Tarò e Val Ceno. *Il Geologo dell'Emilia-Romagna* 22, 15–29 Nuova Serie.
- Settembre Blundo, D., Martin De Vidales, J.L., Alietti, A., 1992. Corrensite-type clay minerals from Taro Valley (North Italy). *Mineralogica et Petrographica Acta* 35, 215–222.
- Sharp, Z.D., Barnes, J.D., 2004. Water-soluble chlorides in massive seafloor serpentinites: a source of chloride in subduction zones. *Earth and Planetary Science Letters* 226, 243–254.
- Siever, R., Woodford, N., 1979. Dissolution kinetics and the weathering of mafic minerals. *Geochimica et Cosmochimica Acta* 43, 717–724.
- Singer, A., 1989. Palygorskite and sepiolite group minerals. In: Dixon, J.B., Weed, S.B. (Eds.), *Minerals in Soil Environments*. Soil Science Society of America, Madison, Wisconsin, pp. 829–872.
- Siffert, B., Wey, R., 1962. Synthèse d'une sepiolite a temperature ordinaire. *Comptes rendus hebdomadaires des séances de l'Académie des Sciences de Paris* 254, 1460–1463.
- Środoń, J., 1999. Nature of mixed-layer clays and mechanisms of their formation and alteration. *Annual Reviews of Earth and Planetary Science* 27, 19–53.
- Stoessell, R.K., 1988. 25 °C and 1 atm dissolution experiments of sepiolite and kerolite. *Geochimica et Cosmochimica Acta* 52, 365–374.
- Stoessell, R.K., Hay, R.L., 1978. The geochemical origin of Sepiolite and keorilite at Amboseli, Kenya. *Contributions to Mineralogy and Petrology* 65, 255–267.
- Suarez, D.L., Šimunek, J., 1996. Solute transport modeling under variably saturated water flow conditions. In: Lichtner, P.C., Steefel, C.I., Oelkers, E.H. (Eds.), *Reactive Transport in Porous Media*. Reviews in Mineralogy, vol. 34. Mineralogical Society of America, Michigan. Book Crafters, Inc. 229–268.
- Sumner, D.Y., Grotzinger, J.P., 1996. Were kinetics of Archean calcium carbonate precipitation related to oxygen concentration? *Geology* 24, 119–122.
- Su, C., Suarez, D.L., 2004. Boron release from weathering of illites, serpentine, shales, and illitic/palygorskitic soils. *Soil Science Society of America Journal* 68, 96–105.
- Toscani, L., Venturelli, G., Boschetti, T., 2001. Sulfide-free and sulfide-bearing waters in the Northern Apennines Italy: general features and water–rock interaction. *Aquatic Geochemistry* 7, 195–216.
- Treves, B.E., Harper, G.D., 1994. Exposure of serpentinites on the ocean floor: sequence of faulting and hydrofracturing in the Northern Apennine ophiolites. *Ophiolite* 19b, 435–466.
- Varadachari, C., Kudrat, M., Gosh, K., 1994. Evaluation of standard free energies of formation of clay minerals by an improved regression method. *Clays and Clay Minerals* 42, 298–307.
- Veniale, F., 1966. Sepiolite in sedimenti dell'Appennino Vogherese (Pavia). *Periodico di Mineralogia* 35, 343–386.
- Venturelli, G., 2003. Acque, minerali ed ambiente — Fondamenti di geochimica dei processi di bassa temperatura. Pitagora Editrice, Bologna.
- Venturelli, G., Contini, S., Bonazzi, A., Mangia, A., 1997. Weathering of ultramafic rocks and element mobility at Mt. Prinzera, Northern Apennines, Italy. *Mineralogical Magazine* 61, 765–778.
- Venturelli, G., Frey, M., 1977. Anchizone metamorphism in sedimentary sequences of the Northern Apennines. *Rendiconti Società Mineralogica Italiana* 33, 109–123.
- Vieillard, P., 2002. A new method for the prediction of Gibbs free energies of formation of phyllosilicates (10 Å and 14 Å) based on the electronegativity scale. *Clays and Clay Minerals* 50, 352–363.
- Vissers, R.L.M., Strating, E.H.H., 2001. Structures and microstructures in a thrust-related, greenschist facies tectonic melange, Voltri Group (NW Italy). *Ophiolite* 26, 33–46.
- Viti, C., Mellini, M., 1997. Contrasting chemical compositions in associated lizardite and chrysotile in veins from Elba, Italy. *European Journal of Mineralogy* 9, 585–596.
- Viti, C., Mellini, M., 1998. Mesh textures and bastites in the Elba retrograde serpentinites. *European Journal of Mineralogy* 10, 1341–1359.
- Wenner, D.B., Taylor Jr., H.P., 1974. Deuterium/atomic hydrogen and oxygen-18/oxygen-16 studies of serpentinization of ultramafic rocks. *Geochimica et Cosmochimica Acta* 38, 1255–1286.
- Williams, L.A., Parks, G.A., Crerar, D.A., 1985. Silica diagenesis I. Solubility controls. *Journal of Sedimentary Petrology* 55, 301–311.
- Wilson, J., Savage, D., Cuadros, J., Shibata, M., Ragnarsdottir, K.V., 2006. The effect of iron on montmorillonite stability. (I) Background and thermodynamic considerations. *Geochimica et Cosmochimica Acta* 70, 306–322.
- Wollast, R., Mackenzie, F.T., Bricker, O.P., 1968. Experimental precipitation and genesis of sepiolite at earth-surface conditions. *American Mineralogist* 53, 1645–1662.
- Wruicke, C.T., 1996. Serpentine and carbonated-hosted asbestos deposits. In: Edward, A., du Bray (Eds.), *Preliminary compilation of descriptive geoenvironmental mineral deposit models, 95–831*. U.S. Geological Survey Open-File Report, pp. 39–46.
- Xu, T., Apps, J.A., Pruess, K., 2001. Analysis of mineral trapping for CO₂ disposal in deep aquifers. Lawrence Berkeley National Laboratory. University of California.
- Zhang, Y., Dawe, R.A., 2000. Influence of Mg²⁺ on the kinetics of calcite precipitation and calcite crystal morphology. *Chemical Geology* 163, 129–138.
- Zhu, C., Anderson, G., 2002. Environmental applications of geochemical modeling. Cambridge University Press.